THE JOURNAL OF PHYSICAL CHEMISTRY B
A JOURNAL OF THE AMERICAN CHEMICAL SOCIETY

pubs.acs.org/JPCB
Article

Nickel-Dithiolene Cofactors as Electron Donors and Acceptors in Protein Hosts

Georgia Polycarpou and Spiros S. Skourtis*

Cite This: J. Phys. Chem. B 2025, 129, 2992−3006
Read Online

ACCESS | Metrics & More | Article Recommendations | Supporting Information

ABSTRACT: Metal dithiolene compounds are attracting considerable attention in the field of molecular electronics, particularly as constituents of materials with high charge-carrier mobilities. Recent experiments on cable bacteria that perform centimeter-scale charge transport suggest that Ni-bis(dithiolene) cofactors are important components of the bacterial conductive network. Further, current−voltage experiments of cable-bacteria-conductive sheaths have measured high conductivity values as compared to other electron-transfer bacteria. An important question is how the Ni-bis(dithiolene) structures participating as electron donors/acceptors contribute to the high conductivity. Currently, the protein and cofactor structures of these bacterial networks are largely unknown. Given this limitation, in this work, we explore the more general question of how Ni-bis(dithiolene) molecules would perform as electron donor and acceptor centers in protein-mediated charge transfer. Our aim is to deduce order-of-magnitude higher bounds for charge-transfer rates in such systems as a function of donor−acceptor distance, protein-bridge (amino acid) sequence, cofactor size, and redox state. These bounds are useful for predicting charge-transfer mechanisms and estimating rates in the absence of detailed structural information on protein wires that may use Ni-bis(dithiolene) redox cofactors. Our analysis is also relevant to the design of artificial Ni-bis(dithiolene) protein wires.

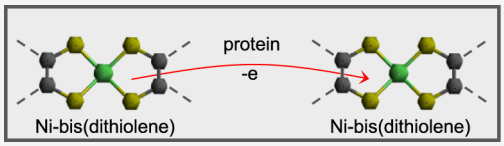

INTRODUCTION

Cable bacteria can transfer electrons along multicellular filaments over centimeter distances. These filaments are often found in marine sediments and they couple, via charge-transport, hydrogen-sulfide oxidation at one end of the filament, inside the sediment, to oxygen reduction at the other end in the sediment-water boundary.[1,2] The conductance of cable-bacteria was studied using two-probe and four-probe current−voltage experiments in which isolated fiber sheaths, which contain the conductive network, were placed on silicon substrates patterned with gold electrodes. Currents were measured as a function of voltage and temperature for sheaths of variable lengths (micrometer to millimeter). The measured room-temperature conductivities were found to be in the range of 0.1−100 S/cm over 1−100 μm distances.[3−11] The maximum conductivity values are high compared to those of other electron transfer bacteria, eg., refs[12−17]. Estimates of cofactor-to-cofactor charge-transfer rates obtained from fitting to these experiments give 0.1−1 psec^{-1} rates for conductivities of 0.1 S/cm (and from estimates of the cofactor center-to-center distances in the range of 0.26−3.3 nm.[9] Raman-spectroscopy studies by Smets et al.[18] indicated that the charge conduction in cable bacteria may involve sulfur-coordinated nickel (Ni) cofactors with Raman spectra similar to Ni-bis(dithiolene) complexes.[6,19] The precise molecular structure of these planar Ni-bis(dithiolene) cofactors in cable bacteria remains unknown. However, many such types of structures have been explored in synthetic systems, and those include single and multinickel bis(dithiolene) complexes.[20−22]

Metal-dithiolene molecules are being studied in the field of molecular electronics[20] with the purpose of building devices having high-carrier mobilities and Seebeck coefficients.[21,23,24] The sulfur ligands of the Ni-bis(dithiolene) group are noninnocent ligands,[25] and the HOMO and LUMO orbitals are known to contain considerable sulfur character in addition to metal.[26−30] Due to the noninnocence of the ligands, it is possible to tune the redox properties of the molecules by ligand substitutions that affect the frontier orbital energetics and delocalization. Further, when such structures are placed in stacked geometries that strongly couple the frontier orbitals of adjacent monomers, the measured conductivities can be 10−100 S/cm.[20−22]

In this work, we do not consider such stacked architectures of Ni-bis (dithiolene) cofactors but rather study isolated cofactors connected to each other by a protein bridge that acts as a charge-transfer mediator (Figure 1). This type of assembly is the most common in biological electron transfer chains and it is the basic pattern for the design of biomolecular wires that perform metal-to-metal protein-mediated electron transfer. The main question we address is the following: given a donor and acceptor that are Ni-bis(dithiolene) cofactors connected

Received: December 6, 2024
Revised: February 10, 2025
Accepted: February 14, 2025
Published: March 6, 2025

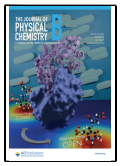

https://doi.org/10.1021/acs.jpcb.4c08264
J. Phys. Chem. B 2025, 129, 2992−3006

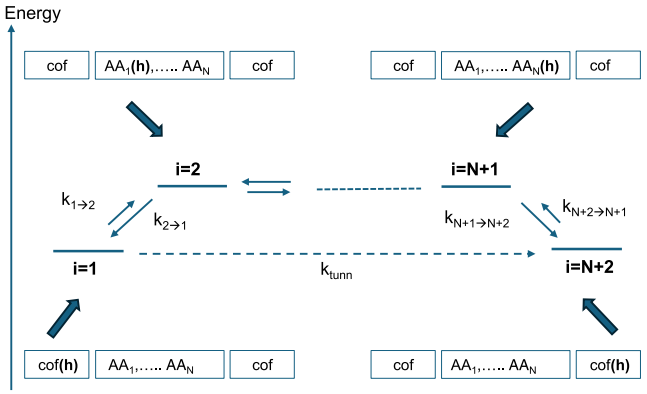

Figure 1. Schematic diagram showing the model of cofactor-to-cofactor hole transfer, mediated either by hopping through real AA intermediates ($k_{i,i\pm1}$ rates), or by tunneling through virtual AA intermediates (k_{tunn} rate).

by an intervening protein bridge, what is the upper bound for the donor-to-acceptor charge transport rate as a function of distance, cofactor size, and cofactor redox state? This question is relevant to understanding the redox function of such cofactors in cable bacteria, but it is also important in the context of designing artificial biomolecular wires with tunable conductivities. As mentioned above the noninnocence of the ligands enables a high degree of control of the reduction potentials. For example, electrochemical experiments of Ni-bis(dithiolene) cofactors with different ligand substitutions show a large variety of oxidation states and reduction potentials (the oxidation states usually vary from +1 to −3). Another feature of such molecules is their square-planar geometry that could enable extended and variable interactions with adjacent amino acids (including pi-stacking interactions) leading to tunable electronic coupling with the protein bridge. These features imply that such cofactors, when used as redox centers in protein wires, may offer a large degree of design versatility aimed at controlling the charge transport speeds.

Currently, there are no known structures of Ni-bis-(dithiolene)-protein systems, biological or synthetic. Cable bacteria have Ni-bis(dithiolene) cofactor content in the electron transfer chain[6] but atomic-level structural details of the chains do not exist yet. Therefore, our analysis of charge transfer in such systems is necessarily coarse-grained. First, it is necessary to consider a variety of Ni-bis(dithiolene) complexes with measured reduction potentials and known oxidation states. Second, we need to determine the most-likely transport regimes of protein-mediated charge-transfer between cofactor units. This requires that we decide on the amino acid (AA) content of the bridge in order to put bounds on the energy barrier of AA-mediated transport. Since we are interested in estimating upper bounds on transfer rates, we should consider AA's that provide the lowest energy gaps for charge transfer (e.g., Trp, Tyr, His, and Cys).[31] Among these, Trp and Tyr have the lowest ionization potentials, and there is extensive experimental and theoretical work showing fast charge transport in biological Trp (Tyr) chains.[32,33] For example, Trp chains are found in photolyases and cryptochromes involved in DNA photorepair and in signal transduction. In these systems, Trp triads transfer a hole from a flavin cofactor over distance of 1.5 nm with nearest-neighbor hopping rates that can be as fast as 1−10 psec.[34−38] It has also been suggested that Trp chains act as efficient escape routes for holes in proteins, rapidly extracting holes that may cause oxidative damage.[31,39−42] Therefore, we consider a Trp (or Tyr) sequence to be the "optimal" bridge from an energetic-barrier point of view for facilitating fast charge transfer (a Tyr sequence would give similar results[43]). In addition, to estimate upper bounds for charge-transfer rates, we also compare reduction potentials of Ni-bis(dithiolene) cofactors to those of common metalloprotein redox cofactors. This comparison is a useful exercise when thinking about the oxidative and reductive roles of these cofactors in biological and biomimetic electron transport chains that contain redox metalloproteins. Further, the reduction potentials are used to predict the direction of spontaneous charge transfer between cofactors and metal leads.

THEORETICAL METHODS

The cofactor structures considered in this work are listed in Figures 2−4. The approximate oxidation states of nickel in Ni-bis(dithiolene) structures with a single nickel atom have been studied previously, and it was shown that there is an approximate correspondence between the formal nickel oxidation state and total charge (Ni(IV) corresponds to total charge 0, Ni(III) to total charge −1, Ni(II) to total charge −2, and Ni(I) to total charge −3).[19,26,28,30] We follow this scheme in our study for the structures in Figures 2−4, i.e. we do not describe the oxidation states of the molecules by using a formal nickel oxidation state, but rather by the total charge on the molecule.

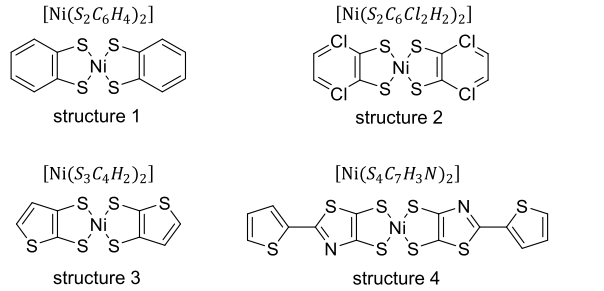

Figure 2. Cofactor structures used in our computations. Structures 1−4 are 1-nickel-4-sulfur (Ni-4S) core structures chosen because there are voltametric measurements of their reduction potentials for different redox states.

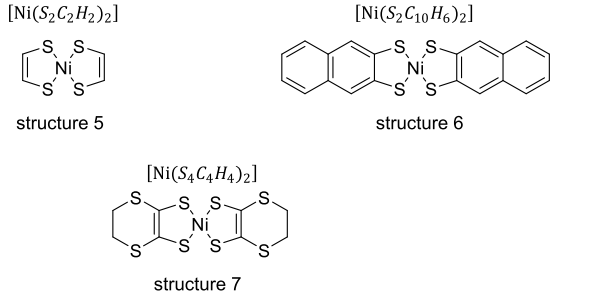

Figure 3. Cofactor structures used in our computations. Structures 5−7 are 1-nickel-4-sulfur (Ni-4S) core structures used to explore the effect of adding different side groups on the redox energies of the core unit.

In the following, cofactor-to-cofactor hole transfer (ht) that is protein-mediated is defined as the process: $cof^{(ox)}$ prot cof → cof $prot^{(ox)}$ cof → cof prot $cof^{(ox)}$, where (ox) denotes oxidized species and $prot^{(ox)}$ denotes cationic AA intermediates (Figure

https://doi.org/10.1021/acs.jpcb.4c08264
J. Phys. Chem. B 2025, 129, 2992−3006

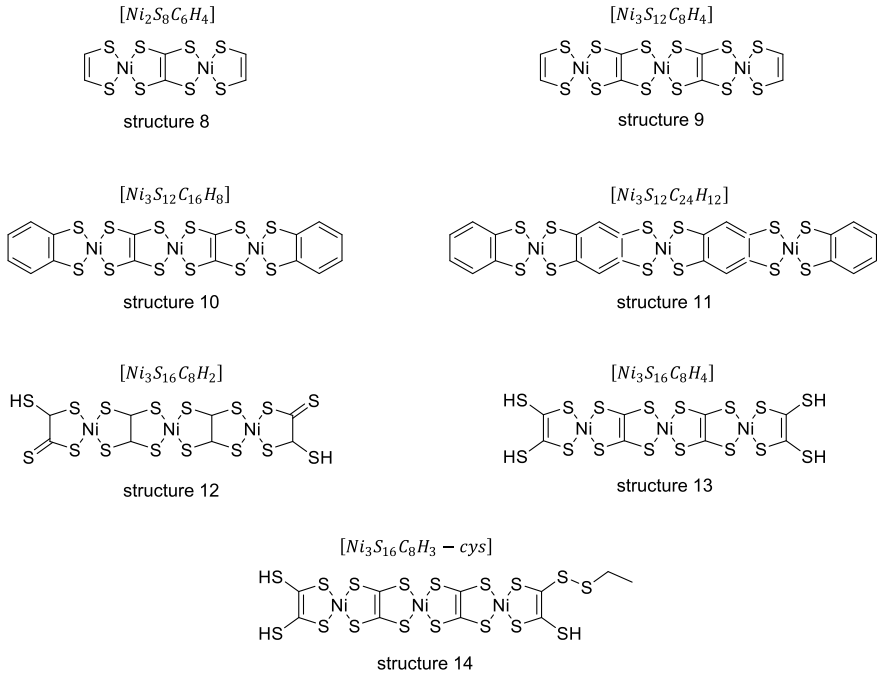

Figure 4. Cofactor structures used in our computations. Structures 8−14 are 2-nickel and 3-nickel structures. Structures 8 and 9 contain the 2-nickel and 3-nickel motifs, respectively, with hydrogen ending groups. Structures 10−14 are the 3-nickel motifs with aromatic rings, sulfur, and cysteine as ending groups.

1). The analogous electron transfer (et) process is defined as: $\mathrm{cof}^{(\mathrm{red})}$ prot cof → cof $\mathrm{prot}^{(\mathrm{red})}$ cof → cof prot $\mathrm{cof}^{(\mathrm{red})}$, where (red) denotes the reduced species and $\mathrm{prot}^{(\mathrm{red})}$ denotes anionic AA intermediates. The case of anionic AA intermediates is very uncommon in biomolecular charge transfer and is considered in the Supporting Information.

The energy gaps for ht are approximated using the following formula:

$$\begin{aligned}\Delta E^{\mathrm{ht}}_{\mathrm{cof}\to\mathrm{AA}} &= [E^{\mathrm{cof}}_{\mathrm{min}}(N_e+1) - E^{\mathrm{cof}}_{\mathrm{min}}(N_e)] + [E^{\mathrm{AA}}_{\mathrm{min}}(M_e-1) - E^{\mathrm{AA}}_{\mathrm{min}}(M_e)] \\ &= -\,\mathrm{EA}^{\mathrm{cof}}_{\mathrm{adiab}}(N_e) + \mathrm{IP}^{\mathrm{AA}}_{\mathrm{adiab}}(M_e) = -\mathrm{IP}^{\mathrm{cof}}_{\mathrm{adiab}}(N_e+1) + \mathrm{IP}^{\mathrm{AA}}_{\mathrm{adiab}}(M_e)\end{aligned} \tag{1}$$

In the equations above, N_e and M_e denote the number of cofactor and AA electrons, respectively, prior to charge transfer. E_{min} denotes the (minimum) energy of the geometry-optimized structure, $\mathrm{IP}_{\mathrm{adiab}}$ and $\mathrm{EA}_{\mathrm{adiab}}$ are adiabatic ionization potentials and electron affinities, estimated from computations on the isolated cofactor and AA structures.[44] The final equation is obtained by noting $\mathrm{EA}_{\mathrm{adiab}}(N_e) = \mathrm{IP}_{\mathrm{adiab}}(N_e+1)$. In our computations, the oxidation states of the AA side chains are allowed to vary between 0 and +1. The oxidation states of the Ni-bis(dithiolene) cofactors as observed in electrochemical experiments are more variable, often ranging from +1 to −3 (e.g., refs 30, 45, and 46 and references therein). In the main text, we focus on cofactor redox couples 0/−1 and −1/−2 that are most commonly observed in electrochemical experiments of Ni-bis(dithiolene) compounds, (e.g., refs 30, 45, and 46) and on the couple +1/0 that is mostly observed for delocalized systems.[45,47−49] The couple −2/−3 is considered in the Supporting Information. Further, as we do not have any structural information about the protein−cofactor environment, we vary the dielectric constant in our computations of the cofactor from $\epsilon = 5$ to $\epsilon = 25$, a range considered to be representative of proteins.[50] Our results are compared to experimental data and previous computations. Large positive values of $\Delta E^{\mathrm{ht}}_{\mathrm{cof}\to\mathrm{AA}}(\Delta E^{\mathrm{et}}_{\mathrm{cof}\to\mathrm{AA}}) \gg K_BT$ would indicate that the protein is insulating for cofactor-to-cofactor charge transfer, providing virtual AA intermediates. In the opposite limit, $\Delta E^{\mathrm{ht}}_{\mathrm{cof}\to\mathrm{AA}}(\Delta E^{\mathrm{et}}_{\mathrm{cof}\to\mathrm{AA}}) < K_BT$ would mean that the AA's may participate as real intermediates in near-resonant or resonant transfer.

In the following, we simplify the notation in eq 1 by replacing the total number of electrons with the total charge. Therefore, $IP^{\mathrm{AA}}_{\mathrm{adiab}}(M_e)$ is denoted as $\mathrm{IP}^{\mathrm{AA}}_{\mathrm{adiab}}(0)$ since we are only considering the AA redox couple +1/0. Further, (N_e) and $(N_e + 1)$ in eq 1 are replaced by (q) and $(q - 1)$ respectively, where q denotes the total charge on the cofactor prior to charge transfer (for the cofactor redox couple +1/0: $q = +1$, for the cofactor redox couple 0/−1: $q = 0$ and for the couple −1/−2: $q = -1$). Using the new notations, the last expression in eq 1 is written as,

$$\Delta E^{\mathrm{ht}}_{\mathrm{cof}\to\mathrm{AA}} = -\mathrm{IP}^{\mathrm{cof}}_{\mathrm{adiab}}(q-1) + \mathrm{IP}^{\mathrm{AA}}_{\mathrm{adiab}}(0) \tag{2}$$

We also use the cofactor $\mathrm{IP}_{\mathrm{adiab}}$ values to estimate the cofactor reduction potentials so as to compare with the potentials of common biological redox cofactors (e.g., hemes, iron−sulfur centers, and blue-copper centers). From this comparison, we can deduce possible oxidative (reducing) roles of the cofactors in the context of biological electron-transfer chains. In addition, from the $\mathrm{IP}_{\mathrm{adiab}}$ values, we estimate thermodynamic energy barriers for hole (electron) injection from a metal to a cofactor (under zero bias and assuming that metal and cofactor are not in direct contact). This information is relevant for electrochemical and molecular junction experiments. The energy barrier for hole injection from a metal with Fermi energy $E^{\mathrm{metal}}_{\mathrm{Fermi}}$ to a cofactor that has total charge q prior to hole injection, is given by,

https://doi.org/10.1021/acs.jpcb.4c08264
J. Phys. Chem. B 2025, 129, 2992−3006

$$\Delta E^{\mathrm{ht}}_{\mathrm{metal}\rightarrow\mathrm{cof}}(\mathrm{cof}:\ q-1\rightarrow q) = -|E^{\mathrm{metal}}_{\mathrm{Fermi}}| + \mathrm{IP}^{\mathrm{cof}}_{\mathrm{adiab}}(q) \tag{3}$$

Electron injection is discussed in the Supporting Information.

We use quantum nonadiabatic Marcus theory to model the hole transport between individual Ni-bis(dithiolene) cofactor units connected by a protein medium. The theory is applicable to most of the systems that we will study. In modeling the protein-mediated cofactor-to-cofactor hole-transfer time scale, the donor-bridge-acceptor unit is represented as a linear hopping network, where the first ($i = 1$) and final ($i = N + 2$) hopping sites are cofactors and the intermediate ones are AA's (Figure 1). The hole-transfer rate from hopping site i to hopping site $i + 1$ is given by,

$$k_{i\rightarrow i+1} = \frac{2\pi}{\hbar}(V_{\mathrm{D}_i\mathrm{A}_{i+1}})^2 \mathrm{FC}_{\mathrm{quant}}(\Delta E_{i+1,i})$$

$$\mathrm{FC}_{\mathrm{quant}}(\Delta E_{i+1,i}) = \frac{1}{2\pi\hbar}\int_{-\infty}^{\infty} \mathrm{d}t \exp(-it\Delta E_{i+1,i}/\hbar) \exp(-G_{i,i+1}(0) + G_{i,i+1}(t))\exp(-\Gamma|t|). \tag{4}$$

$V_{\mathrm{D}_i\mathrm{A}_{i+1}}$ is the electronic coupling between the site i donor state (D_i) and the site $i + 1$ acceptor state (A_{i+1}). $\mathrm{FC}_{\mathrm{quant}}(\Delta E_{i+1,i})$ is the quantum Franck–Condon factor, where $\Delta E_{i+1,i}$ is the energy gap of the reaction $\mathrm{D}_i^+\mathrm{A}_{i+1} \rightarrow \mathrm{D}_i\mathrm{A}_{i+1}^+$,

$$\Delta E^{\mathrm{ht}}_{i+1,i} = (E^{\mathrm{min}}_{\mathrm{D}} + E^{\mathrm{min}}_{\mathrm{A}^+}) - (E^{\mathrm{min}}_{\mathrm{D}^+} + E^{\mathrm{min}}_{\mathrm{A}}) = -(\mathrm{IP}_{\mathrm{D}})_{\mathrm{adiab}} + (\mathrm{IP}_{\mathrm{A}})_{\mathrm{adiab}} \tag{5}$$

Γ in eq 4 is the vibrational relaxation rate (leading to a homogeneous broadening width of the normal mode vibrational states). For a voltage bias ΔV along the $N + 2$ - site chain, ΔE_{i+1} is replaced by $\Delta E^{\mathrm{bias}}_{i+1,i} = \Delta E_{i+1,i} - |e|\Delta V/(N+1)$, i.e., we assume a linear voltage-bias profile. In eq 4, $G_{i,i+1}(t) = G_{\mathrm{D}}(t) + G_{\mathrm{A}}(t)$ with

$$G_{\mathrm{D}}(t) = \sum_{\alpha}\frac{\lambda_\alpha}{\hbar\omega_\alpha}\left[(2\langle n_\alpha\rangle + 1)\cos(\omega_\alpha t) - i\sin(\omega_\alpha t)\right]$$

$$G_{\mathrm{A}}(t) = \sum_{\beta}\frac{\lambda_\beta}{\hbar\omega_\beta}\left[(2\langle n_\beta\rangle + 1)\cos(\omega_\beta t) - i\sin(\omega_\beta t)\right] \tag{6}$$

In the equation above, α (β) are normal mode indices for the D (A) molecules. $\lambda_{\alpha(\beta)}$ denotes the inner-sphere reorganization energy of a normal mode with frequency $\hbar\omega_{\alpha(\beta)}$ upon oxidation or reduction of D (or A). $\langle n_{\alpha(\beta)}\rangle = (\exp(\hbar\omega_{\alpha(\beta)}/K_{\mathrm{B}}T) - 1)^{-1}$ is the mean occupation number of the normal mode, at temperature T. For the amino acid Trp, Figure S1 shows the electron–phonon couplings per mode, $\lambda_\alpha/\hbar\omega_\alpha$, as a function of each normal mode energy, $\hbar\omega_\alpha$, that enter in the computation of the quantum Franck–Condon factor.

Given the choice of cofactors for initial donor $i = 1$ and final acceptor $i = N + 2$, and the choice of AA sequence for the protein-bridge $i = 2 - N + 1$, we estimate the energy gaps in eq 5 for each hopping pair (i, $i + 1$) from the ab initio computations and experimental reduction potential data (see below). Further, we compute at the ab initio level all the normal-mode frequencies and reorganization energies needed in eq 6 using the isolated molecules of sites i and $i + 1$ (for AA's, the molecule is the capped side chain). In our computations, the electronic coupling $V_{\mathrm{D}_i\mathrm{A}_{i+1}}$ is a variable parameter because it depends on the secondary and tertiary structure of the cofactor-protein system. We deduce maximum values by reference to biological AA chains where such matrix elements have been computed and by performing ab initio coupling computations between the cofactors and AA side chains for different geometries (Supporting Information).

Having obtained a set of values for the above quantities, we compute all $k_{i\rightarrow i\pm1}$ by first computing the Franck–Condon factor $\mathrm{FC}_{\mathrm{quant}}(\Delta E_{i\pm1,i})$ via the Fourier transform in eq 4. From the $k_{i\rightarrow i\pm1}$ we build an $(N + 2) \times (N + 2)$ rate matrix $\tilde{K}$ and solve the differential equations for the hopping-site occupation probabilities $P_i(t)$. Denoting by $\vec{P}(t)$ the $(N + 2) \times 1$ vector of $P_i(t)$, the differential equations are written as $\mathrm{d}\vec{P}(t)/\mathrm{d}t = \tilde{K}\vec{P}(t)$ and their solutions are given by,

$$\vec{P}(t) = \sum_{j=1}^{N+2}\vec{X}_j^R\left(\frac{\vec{X}_j^L\cdot\vec{P}(t=0)}{\vec{X}_j^L\cdot\vec{X}_j^R}\right)\exp(s_j t) \tag{7}$$

$\vec{X}_j^L$ and $\vec{X}_j^R$ are the left and right eigenvectors ($1 \times (N + 2)$ and $(N + 2) \times 1$) of the rate matrix $\tilde{K}$ with eigenvalue s_j. We deduce the cofactor-to-cofactor hole-transfer rate mediated by the protein $1/\tau_{1\rightarrow N+2}$, by setting $P_i(t = 0) = \delta_{i,1}$ and following the time evolution of the final-site probability $P_{N+2}(t)$.

COMPUTATIONAL METHODS

Estimation of Energy Gaps for Cofactor-to-AA Electron and Hole Injection. We perform geometry optimizations without symmetry constraints on the cofactors in Figures 2–4 using density functional theory (DFT) with the BP86 functional[51,52] and the ZORA-def2-TZVP basis set,[53,54] as implemented in ORCA-5.0.1 software package.[55,56] This functional has previously shown to perform well for first row (3d-series) transition metal complexes (e.g., Ni).[19,28,57−59] Scalar relativistic effects are included in the context of zeroth-order regular approximation (ZORA).[60] We perform both restricted closed-shell and open-shell computations. Most of the even electron systems (total charge equal to 0 or −2) are singlets, and a few are triplets. The odd electron systems (total charge equal to +1, −1, and −3) are doublets. Doing a higher level of theory such as multiconfigurational computations that are sometimes required in dithiolene systems (e.g., refs28,[61−63]), will not provide further insight given that we do not know how these systems are bonded to the protein environment nor do we know the protein environment. For AA's (phenylalanine, tyrosine, tryptophan, cysteine, and histidine) we use the BHandHLYP functional[64,65] combined with the def2-TZVP basis set.[53] To probe solvent effects on energetics, we use the Conductor-like Continuum Polarization Model (C-PCM)[66] with different dielectric constants ($\epsilon \approx 5$, 25) corresponding to the protein interior and exterior environments.[50]

Estimation of Inner-Sphere Reorganization Energies of Cofactors and Amino Acid Side Chains. To simulate nonadiabatic rates using a quantum description of the vibrations, we need to compute the quantum Franck–Condon factors for the molecules of the charge-transfer chain (eqs

https://doi.org/10.1021/acs.jpcb.4c08264
J. Phys. Chem. B 2025, 129, 2992−3006

4−6). For each molecule, we compute the normal modes α and their frequencies ω_α for the initial and final charged states of the molecule (before/after charge transfer). The normal modes are used in the FCF (Franck−Condon Factors) auxiliary program[67−69] of the AMS 2023.101 software package[70] to compute the reorganization energy of each mode λ_α, and the total inner-sphere reorganization energy, $\lambda = \sum_\alpha \lambda_\alpha$. The ω_α and λ_α are then used in eqs 4−6. All computations employ the BP86[51,52] functional and the TZ2P basis set within the ZORA approximation[60] for the cofactor structures, and BHandHLYP[64,65] functional with the TZ2P basis set for the AA side chains.

Estimation of Electronic Couplings for Different Ni-Cofactor/Tryptophan Geometries. To approximate maximum values for cofactor-to-aninoacid electronic couplings, we used the fragment approach and the charge-transfer-integral module as implemented in the ADF software package.[70] The first fragment is the Ni-cofactor structure and the second is the AA. The electronic coupling between the orbitals of different fragments is given by,[71,72]

$$V_{i,f} = \frac{J_{i,f} - S_{i,f}(\epsilon_i - \epsilon_f)/2}{1 - S_{i,f}^2} \quad (8)$$

$J_{i,f} = \langle \phi_i | \hat{H}_{KS} | \phi_f \rangle$ is the transfer integral between the initial $|\phi_i\rangle$ and the final $|\phi_f\rangle$ fragment orbitals, where $\hat{H}^{KS}$ is the Kohn−Sham Hamiltonian (we use the BP86[51,52] /TZ2P level of theory). $S_{i,f} = \langle \phi_i | \phi_f \rangle$ is the spatial overlap integral between these fragment orbitals and $\epsilon_{i/f} = \langle \phi_{i/f} | \hat{H}_{KS} | \phi_{i/f} \rangle$ is the energy of the fragment orbital $|\phi_{i/f}\rangle$.

RESULTS AND DISCUSSION

The cofactors used in our computations are shown in Figures 2−4. Figures 2 and 3 show structures with a 1-nickel-4-sulfur (Ni-4S) core and with a variety of ending groups. Figure 4 contains structures with two and three Ni-4S core motifs. Multi-Nickel motifs have been synthesized and used as building blocks of conducting materials[21,22] and should be considered in our analysis. The structures in Figure 2 are chosen because there are voltammetric measurements of their reduction potentials for different redox states. This information allows us to evaluate directly from experiments the charge-transfer properties of these structures within a protein host, and also to gauge our computations against experiments.[30,45,46] The different structures in Figure 3, all with a single Ni-4S core, are used to explore the effect of adding different side groups on the redox energies of the core unit (structure 5: hydrogen side groups; structures 6 and 7: aromatic and sulfur-containing side groups). The multi-Ni structures in Figure 4 also contain different types of side groups (structure 8: two Ni with hydrogen side groups; structures 9−14: three Ni with H, aromatic rings, S−H, or Cys side groups).

Table 1 shows the computed IP^{AA}_{adiab} of different neutral AA side chains in $\epsilon = 5$ and $\epsilon = 25$ (the AA's shown are those with the lowest IP^{AA}_{adiab} energies). The ordering of the IP_{adiab} is consistent with earlier computations of AA ionization potentials, e.g., refs73 and74 and is also consistent with experimental reduction potentials (see below).

We estimate the energy gaps $\Delta E^{ht}_{cof\to AA}$ for cofactor-to-AA hole transfer using eqs 1 and 2 and the computed values of IP^{AA}_{adiab} for each neutral AA and of IP^{cof}_{adiab} for each cofactor in Figures 2−4 (with different cofactor total charges). Similar computations are done for protein-mediated electron transfer (see Supporting Information). For all cofactor structures in Figures 2−4 and for the cofactor redox couple 0/−1, hole transfer is more favorable than electron transfer and they are both endergonic, i.e., $K_BT < \Delta E^{ht}_{cof\to AA} < \Delta E^{et}_{cof\to AA}$. For the redox couple −1/−2, most structures in Figures 2−4 also give $K_BT < \Delta E^{ht}_{cof\to AA} < \Delta E^{et}_{cof\to AA}$ (Section S4). For +1/0, all structures give $\Delta E^{ht}_{cof\to AA} < \Delta E^{et}_{cof\to AA}$. However, for +1/0 there are structures with $\Delta E^{ht}_{cof\to AA} \simeq K_BT$ or $\Delta E^{ht}_{cof\to AA} < 0$. In summary, AA-mediated ht is generally favored over AA-mediated et. We also find that the lowest $\Delta E^{ht}_{cof\to AA}$ gaps involve *Trp*, followed by *His* and *Tyr*. Therefore, we expect that the maximum protein-mediated hole-transfer rate between cofactors would be obtained if the cofactors were electronically coupled via a chain of *Trp*'s.

In the following, we focus our discussion on *Trp*-mediated ht between cofactors. Tables 2−4 show the IP^{cof}_{adiab} and the cofactor-to-Trp energy gaps, $\Delta E^{ht}_{cof\to Trp}$, for all cofactors under

Table 1. Ionization Potential $IP^{AA}_{adiab}(0)$ for Amino Acid Side Chains in Dielectric Constants $\epsilon \approx 5$, 25[a]

	$\epsilon \approx 5$	$\epsilon \approx 25$
amino acid	$IP^{AA}_{adiab}(0)$ (eV)	
Cys	6.99	6.55
Phenyl	6.84	6.50
Tyr	6.20	5.86
His	6.00	5.88
Trp	5.67	5.34

[a]The computations are performed at the BHandHLYP/def2-TZVP,[53,64,65] level of theory using the C-PCM[66] to probe the solvent effects. The ORCA-5.0.1 software package is used.[55,56].

Table 2. Cofactor Ionization Potentials $IP^{cof}_{adiab}(q-1)$ and Energy Gaps $\Delta E^{ht}_{cof\to Trp}$ in Dielectric Constants $\epsilon \approx 5$, 25 (Cofactor Structures in Figures 2−4)[ab]

	$\epsilon \approx 5$		$\epsilon \approx 25$	
cof. str.	$IP^{cof}_{adiab}(0)$(eV)	$\Delta E^{ht}_{cof\to Trp}$(eV)	$IP^{cof}_{adiab}(0)$(eV)	$\Delta E^{ht}_{cof\to Trp}$(eV)
5 in Figure 3	6.39	−0.72	6.09	−0.74
2 in Figure 2	6.27	−0.60	6.03	−0.69
10 in Figure 4	5.97	−0.30	5.80	−0.46
14 in Figure 4	5.78	−0.11	5.62	−0.28
4 in Figure 2	5.65	0.02	5.46	−0.12
11 in Figure 4	5.64	0.03	5.49	−0.14
13 in Figure 4	5.63	0.04	5.46	−0.11
7 in Figure 3	5.38	0.29	5.17	0.17

[a]Data refer to the redox couple +1/0, i.e., q = +1 in eq 2. [b]The computations are performed at the BP86/ZORA-def2-TZVP[51−54] level of theory within the ZORA approximation[60] using the C-PCM[66] to probe the solvent effects. The ORCA-5.0.1 software package is used.[55,56].

https://doi.org/10.1021/acs.jpcb.4c08264
J. Phys. Chem. B 2025, 129, 2992−3006

Table 3. Cofactor Ionization Potentials $IP^{cof}_{adiab}(q-1)$ and Energy Gaps $\Delta E^{ht}_{cof\rightarrow Trp}$ in Dielectric Constants $\epsilon \approx 5, 25$ (Cofactor Structures in Figures 2−4)[ab]

	$\epsilon \approx 5$		$\epsilon \approx 25$	
cof. str.	$IP^{cof}_{adiab}(-1)$(eV)	$\Delta E^{ht}_{cof\rightarrow Trp}$(eV)	$IP^{cof}_{adiab}(-1)$(eV)	$\Delta E^{ht}_{cof\rightarrow Trp}$(eV)
12 in Figure 4	4.95	0.72	5.12	0.23
10 in Figure 4	4.92	0.75	5.12	0.22
11 in Figure 4	4.90	0.77	5.09	0.25
9 in Figure 4	4.80	0.87	5.01	0.34
14 in Figure 4	4.63	1.04	4.81	0.54
13 in Figure 4	4.61	1.06	4.80	0.55
2 in Figure 2	4.54	1.13	4.81	0.54
8 in Figure 4	4.50	1.17	4.75	0.59
6 in Figure 3	4.38	1.29	4.66	0.68
1 in Figure 2	4.20	1.47	4.51	0.84
4 in Figure 2	4.01	1.66	4.29	1.05
3 in Figure 2	3.96	1.71	4.27	1.08
5 in Figure 3	3.88	1.79	4.21	1.14
7 in Figure 3	3.71	1.96	4.03	1.31

[a]Data refer to the redox couple 0/−1, i.e., $q = 0$ in eq 2. [b]The computations are performed at the BP86/ZORA-def2-TZVP[51−54] level of theory within the ZORA approximation[60] using the C-PCM[66] to probe the solvent effects. The ORCA-5.0.1 software package is used.[55,56].

Table 4. Cofactor Ionization Potentials $IP^{cof}_{adiab}(q-1)$ and Energy Gaps $\Delta E^{ht}_{cof\rightarrow Trp}$ in Dielectric Constants $\epsilon \approx 5, 25$ (Cofactor Structures in Figures 2−4)[ba]

	$\epsilon \approx 5$		$\epsilon \approx 25$	
cof. str.	$IP^{cof}_{adiab}(-2)$(eV)	$\Delta E^{ht}_{cof\rightarrow Trp}$(eV)	$IP^{cof}_{adiab}(-2)$(eV)	$\Delta E^{ht}_{cof\rightarrow Trp}$(eV)
12 in Figure 4	4.21	1.46	4.75	0.60
11 in Figure 4	4.12	1.55	4.65	0.70
10 in Figure 4	4.04	1.63	4.62	0.72
14 in Figure 4	3.87	1.80	4.43	0.91
9 in Figure 4	3.86	1.81	4.47	0.87
13 in Figure 4	3.86	1.81	4.41	0.94
8 in Figure 4	3.31	2.36	4.05	1.29
2 in Figure 2	3.01	2.66	3.80	1.54
6 in Figure 3	2.94	2.73	3.72	1.62
4 in Figure 2	2.78	2.89	3.54	1.81
1 in Figure 2	2.66	3.01	3.52	1.83
3 in Figure 2	2.49	3.18	3.36	1.99
7 in Figure 3	2.37	3.30	3.24	2.10
5 in Figure 3	2.19	3.48	3.15	2.19

[a]Data refer to the redox couple −1/−2, i.e., $q = -1$ in eq 2. [b]The computations are performed at the BP86/ZORA-def2-TZVP[51−54] level of theory within the ZORA approximation[60] using the C-PCM[66] to probe the solvent effects. The ORCA-5.0.1 software package is used.[55,56].

study. Table 2 refers to the redox couple +1/0, Table 3 to 0/−1, and Table 4 to −1/−2 (the −2/−3 couple is considered in Table S3). Some observations relating to these data are (a) IP^{cof}_{adiab} increases with increasing dielectric constant for the negatively charged species. (b) Keeping the dielectric constant fixed, we get $IP^{cof}_{adiab}(-3) < IP^{cof}_{adiab}(-2) < IP^{cof}_{adiab}(-1) < IP^{cof}_{adiab}(0)$. Therefore, the $\Delta E^{ht}_{cof\rightarrow Trp}$ are lower for the redox couple +1/0 (as follows from eq 2). (c) Regarding the redox couples 0/−1, −1/−2, the 3-Ni structures 9−14 in Figure 4 have the highest $IP^{cof}_{adiab}(q-1)$ values and the lowest energy gaps, $\Delta E^{ht}_{cof\rightarrow Trp}$, followed by the 2-Ni structure 8 in Figure 4 and the 1-Ni structure 1 in Figure 2, with the aromatic rings. Thus, $\Delta E^{ht}_{cof\rightarrow Trp}$ decreases with the elongation of the molecule for these couples (addition of aromatic groups or of Ni-4S centers).

Comparison with Experiments. To obtain experimentally derived free-energy gaps for ht and to gauge the accuracy of our computations, we also consider several Ni-bis(dithiolene) complexes for which experimental measurements of their reduction potentials are available (Table 5). We denote these potentials $E^{red}_{electrode}$(cof: $q \rightarrow q-1$), (e.g., $q = 0$ for the redox couple 0/−1, $q = -1$ for the redox couple −1/−2 and $q = +1$ for the redox couple +1/0). The experimentally derived reduction potential of Trp^+ vs NHE for protonated Trp^+, denoted E^{red}_{NHE}(Trp: $+1 \rightarrow 0$), is usually in the range of 0.8 V to 1.2 V depending on the pH.[75,76] From these experimental reduction potentials, we approximate the free energy for cofactor-to-Trp hole transfer as follows,

https://doi.org/10.1021/acs.jpcb.4c08264
J. Phys. Chem. B 2025, 129, 2992−3006

Table 5. Reduction Potential for Various Ni-bis(dithiolene) Complexes Obtained from Cyclic Voltammetry Experiments in refs30,45−47,49

	$E^{red}_{Fc^+/Fc}$(V)	
complex	0/−1	−1/−2
$[Ni(S_2C_6H_4)_2]^{aa}$		−0.95
$[Ni(S_2C_6Cl_2H_2)_2]^{aa}$		−0.65
$[Ni(S_3C_4H_2)_2]^{bb}$	−0.21	−1.09
$[Ni(S_4C_7H_3N)_2]^{cc}$	−0.10	−0.86
$[Ni(S_4C_8H_4)_2]^{cc}$	−0.24	−1.00

	E^{red}_{SSCE} (V)		
complex	+1/0	0/−1	−1/−2
$[Ni(S_4C_{10}H_6)_2]^{dee}$	1.08	0.13	−0.66
$[Ni(S_3C_{12}H_8)_2]^{ee}$	1.10	0.05	−0.75
$[Ni(S_2C_{14}Br_2H_8)_2]^{ee}$		0.09	−0.71
$[Ni(S_2C_2Ph_2)_2]^{ee}$		0.12	−0.82

[a]from ref30. [b]from ref45. [c]from ref46. [d]from ref47. [e]from ref49.

$$\Delta G^{ht}_{cof\rightarrow Trp} \simeq -|e|[E^{red}_{electrode}(cof: q \rightarrow q-1) - E^{red}_{electrode}(Trp: +1 \rightarrow 0)] \quad (9)$$

We can also gauge the accuracy of our computed values for IP_{adiab} in different dielectric constants by extracting experimentally derived IP_{adiab} from the reduction potentials. Consider the reduction half-reaction,

$$molec(q) + e^- \rightarrow molec(q-1) \quad (10)$$

where $q-1$ denotes the total charge of the reduced molecule. The relation between the reduction potential of the oxidized molecule and the IP_{adiab} of the reduced molecule is approximately given by,

$$E^{red}_{electrode}(molec: q \rightarrow q-1) \simeq \frac{IP^{molec}_{adiab}(q-1)}{|e|} - \Delta_{electrode} \quad (11)$$

where $\Delta_{electrode} > 0$ is an electrode-specific constant. For the normal hydrogen electrode, we use the value of $\Delta_{NHE} = 4.5$ V.[77] The free energy notation ΔG in eq 9 is used only for experimentally derived energy gaps that naturally involve averages of energy gaps over thermal fluctuations of the molecule(s). In contrast, the energy difference notation, ΔE, in eqs 1−3, is used for energy gaps derived from ab initio single point computations on geomerty-optimized structures in different dielectric constants.

The first set of experiments,[30,45,46] we consider involves the structures shown in Figure 2. The experiments performed voltammetric measurements that observed only the redox couples 0/−1 and −1/−2. For structure 1 in Figure 2, $E^{red}_{Fc^+/Fc}(cof: -1 \rightarrow -2) = -0.95$ V and for structure 2 (halogenated structure 1) in Figure 2, $E^{red}_{Fc^+/Fc}(cof: -1 \rightarrow -2) = -0.65$ V.[30] For structure 3 in Figure 2, $E^{red}_{Fc^+/Fc}(cof: -1 \rightarrow -2) = -1.09$ V and $E^{red}_{Fc^+/Fc}(cof: 0 \rightarrow -1) = -0.21$ V.[45] For structure 4 in Figure 2, $E_{Fc^+/Fc}(cof: -1 \rightarrow -2) = -0.86$ V and $E_{FC^+/Fc}(cof: 0 \rightarrow -1) = -0.10$ V.[46] The replacement of N atoms with CH groups in the two inner thiophene ligands of structure 4 shifts these reduction potentials to $E_{Fc^+/Fc}(cof: -1 \rightarrow -2) = -1.0$ V and $E_{FC^+/Fc}(cof: 0 \rightarrow -1) = -0.24$ V.[46] In summary, in all cases $E_{Fc^+/Fc}(cof: -1 \rightarrow -2) < E_{Fc^+/Fc}(cof: 0 \rightarrow -1)$. We convert the above $E^{red}_{Fc^+/Fc}$ to E^{red}_{NHE} using the formula $E^{red}_{NHE} = E^{red}_{Fc^+/Fc} + \delta$ where $\delta = 0.40-0.60$ V (the range of values reported in the literature[31,78,79]). Using the different δ, we obtain a range of possible $E^{red}_{NHE}(cof: q \rightarrow q-1)$ for each structure. To take into account different solvent environments for Trp, we use the range $E^{red}_{NHE}(Trp: +1 \rightarrow 0) = 0.8 - 1.2$ V.[75,76] Then from eq 9, we estimate a range of possible $\Delta G^{ht}_{cof\rightarrow Trp}$ for each structure.

Following this procedure, the upper and lower values of the estimated $\Delta G^{ht}_{cof\rightarrow Trp}$ for the cofactor structures in Figure 2 in the different redox states are as follows: (a) redox couple 0/−1, minimum $\Delta G^{ht}_{cof\rightarrow Trp} = 0.30$ eV (for structure 4 in Figure 2) and maximum $\Delta G^{ht}_{cof\rightarrow Trp} = 1.01$ eV (for structure 3 in Figure 2). (b) Redox couple −1/−2, minimum $\Delta G^{ht}_{cof\rightarrow Trp} = 0.85$ eV (for structure 2 in Figure 2) and maximum $\Delta G^{ht}_{cof\rightarrow Trp} = 1.89$ eV (for structure 3 in Figure 2). In summary, $\Delta G^{ht}_{cof\rightarrow Trp}(cof: -1 \rightarrow -2) > \Delta G^{ht}_{cof\rightarrow Trp}(cof: 0 \rightarrow -1)$. This trend is also seen in our ab initio computations of $\Delta E^{ht}_{cof\rightarrow Trp}$. The computational values are closer to the experimental ones for $\epsilon = 25$, and overestimate the experimental values by 0.04−0.80 eV. This is expected since the adiabatic IP differences can only be a very qualitative proxy to reduction potential differences.

The second set of experiments we consider involve voltametric measurements that observe the redox couple +1/0, in addition to −1/−2 and 0/−1, for the same Ni-bis(dithiolene) structure.[47−49] The redox couple +1/0 is less common[45] and it is observed for structures having high delocalization due to fused rings or extended aryl groups (such as the molecules in refs[47−49]). Due to the flexibility of these molecules, it is impossible to predict, via ab initio computations on the isolated molecule, the conformation within a protein host and the corresponding IP^{cof}_{adiab}. Thus, we use these experiments to obtain experimentally derived free energy gaps for ht in the case of the +1/0 couple and to compare them to the −1/−2 and 0/−1 free-energy gaps for the same structures. The experimentally derived $E^{red}_{NHE}(cof: q \rightarrow q-1)$ are in the ranges: $E^{red}_{NHE}(cof: -1 \rightarrow -2)$: (−0.60) − (−0.40) V, $E^{red}_{NHE}(cof: 0 \rightarrow -1)$: 0.15−0.40 V, $E^{red}_{NHE}(cof: +1 \rightarrow 0)$: 1.25−1.35 V. In all cases, $E^{red}_{NHE}(cof: -1 \rightarrow -2) < E^{red}_{NHE}(cof: 0 \rightarrow -1) < E^{red}_{NHE}(cof: +1 \rightarrow 0)$. Using these values in eq 9, we get: $\Delta G^{ht}_{cof\rightarrow Trp}(cof: -1 \rightarrow -2) = 1.21-1.99$ eV, $\Delta G^{ht}_{cof\rightarrow Trp}(cof: 0 \rightarrow -1) = 0.42-1.29$ eV and $\Delta G^{ht}_{cof\rightarrow Trp}(cof: +1 \rightarrow 0) = (-0.55)-(0.19)$ eV. Thus, $\Delta G^{ht}_{cof\rightarrow Trp}(cof: -1 \rightarrow -2) > \Delta G^{ht}_{cof\rightarrow Trp}(cof: 0 \rightarrow -1) > \Delta G^{ht}_{cof\rightarrow Trp}(cof: +1 \rightarrow 0)$. The ordering is consistent with our ab initio computations on the different structures (Tables 2−4), and with the first set of experiments that involve the 0/−1 and −1/−2 couples. The most important observation is that the free-energy gaps for cofactor-to-protein hole injection involving the cofactor redox couple +1/0 are very low compared with the other redox couples. Hole injection to Trp can even be exothermic for the redox couple +1/0 (see Figure 5).

https://doi.org/10.1021/acs.jpcb.4c08264
J. Phys. Chem. B 2025, 129, 2992−3006

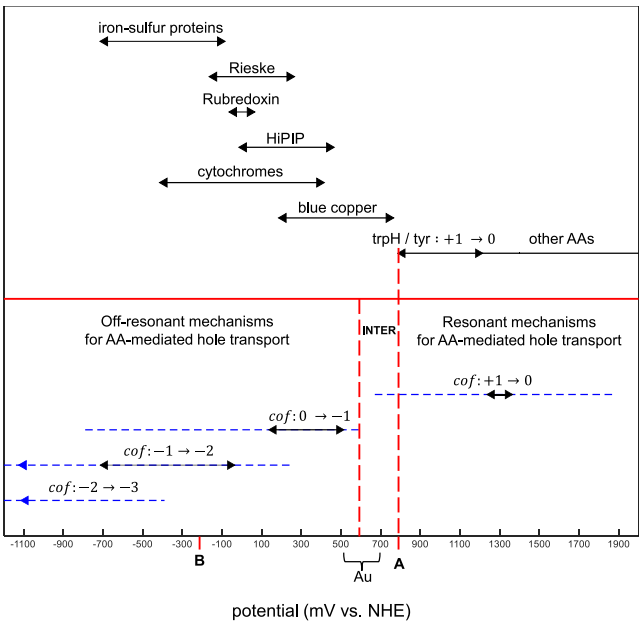

Figure 5. Upper panel: approximate ranges of reduction potential vs NHE (E^{red}_{NHE} in mV) of different metal redox cofactors involved in biological charge-transfer chains,[80] and of amino acids such as protonated *Trp*$^{+}$.[75,76] Lower panel: approximate reduction potential ranges for different Ni-bis(dithiolene) cofactors. The solid-black lines represent ranges measured in experiments.[30,45−49] The blue-dashed lines are extensions of the ranges as predicted from our ab initio computations of the IP^{cof}_{adiab} values for the structures in Figures 2−4 (in combination with eq 11). Also shown along the x axis are (1) the approximate range of the reduction potential for gold (Au),[84,85] (2) the approximate standard reduction potential of O_2 for pH = 7 for the half reaction $(1/2)O_2 + 2H^+ + 2e^- \rightarrow H_2O$ (point A at 0.8 V), (3) the approximate standard reduction potential at pH = 7 for the half reaction $S + 2H^+ + 2e^- \rightarrow H_2S$ (point B at −0.2 V).[81,82] The redox couple −2/−3 has the most negative potentials. The potential of the redox couple +1/0 may overlap with those of some amino acids, leading to resonant transport mechanisms for protein-mediated transport. The other redox couples, having more negative potentials, support off-resonant transport mechanisms. In the intermediate transport regime (labeled INTER) the mechanism (resonant or off-resonant) depends critically on the rms D(A)-bridge coupling.

Comparison Between Ni-bis(dithiolene) Cofactors and Other Metalloprotein Cofactors. At this point, it is useful to compare all the experimentally derived $E^{red}_{NHE}(\text{cof: } q \rightarrow q-1)$ values,[30,45−49] and the values derived from computations, to the E^{red}_{NHE} of some metalloprotein redox centers[80] (Figure 5). The approximate ranges of E^{red}_{NHE} for redox metalloproteins are (−0.4) − 0.4 V (cytochromes), 0.2−0.75 V (blue copper), and (−0.7) − (−0.1) V for most iron−sulfur proteins apart from Rubredoxin (−0.05) − 0.05 V, Rieske (−0.15) − 0.25 V, and HiPIP 0−0.45 V.[80] For the cofactors $E^{red}_{NHE}(\text{cof: } -1 \rightarrow -2)$: (−0.70) − (−0.05)V, $E^{red}_{NHE}(\text{cof: } 0 \rightarrow -1)$: (0.15) − (0.5)V, and $E^{red}_{NHE}(\text{cof: } +1 \rightarrow 0)$: (1.25) − (1.35)V. Therefore, the redox couple −1/−2 with negative E^{red}_{NHE} has high E^{red}_{NHE} overlap with all the negative-potential metalloproteins. The couple 0/−1 with more positive E^{red}_{NHE} has high overlap with the positive ranges of Rieske protein, HiPIP, and some cytochromes, and with the lower range of blue copper proteins. Thus, for the redox couples −1/−2 and 0/−1, the protein presents an energy barrier for hole transfer even for aromatic AA's such as Trp and Tyr. Regarding our ab initio computations, the lower barriers among these couples are for 0/−1 and for extended structures (the 3-Ni structure 12 in Figure 4 has the lowest $\Delta E^{ht}_{cof\rightarrow Trp} = 0.23$ eV for $\epsilon = 25$). In contrast, for the less common +1/0 redox couple, $E^{red}_{NHE}(\text{cof: } +1 \rightarrow 0)$ is the most positive and may overlap with copper proteins and the lowest AA potentials (such as Trp and Tyr). The implication is that $\Delta E^{ht}_{cof\rightarrow Trp}$ can be less than K_BT and even negative. Thus, protein-mediated ht involving the cofactor redox couple +1/0 is not necessarily endergonic.

Figure 5 also shows the approximate standard reduction potential vs NHE at pH = 7 for the half reaction $(1/2)\ O_2 + 2H^+ + 2e^- \rightarrow H_2O$, (point A at 0.8 V), and the standard reduction potential at pH = 7 for the half reaction $S + 2H^+ + 2e^- \rightarrow H_2S$ (point B at −0.2 eV).[81−83] Point A indicates that all of the studied cofactor structures for the redox couples −3/−2, −2/−1, and −1/0 can reduce O_2, i.e., their reduction potentials are more negative than that of point A, falling within a window consistent with physiological redox chains that reduce O_2. The only exception is the redox couple +1/0, for which only some of the structures with the least positive reduction potentials (below point A) could reduce O_2. Therefore, many Ni-bis(dithioline) structures may be used in protein wires as intermediate redox cofactors for O_2 reduction. Point B is relevant to cable bacteria that oxidize H_2S to reduce O_2 following charge transfer (the reduction potential of the half reaction in the bacterial environment could be as low as −0.4 V[82]). Thus, the redox couples/structures that are compatible with cable-bacteria biological redox function lie within the approximate B−A window. From the figure, we see that the redox couple −2/−3 is less likely to accept electrons from oxidized H_2S as its redox potentials are below point B.

Cofactor-to-Metal Hole-Injection Energy Gaps. Using the computed $IP^{cof}_{adiab}(q)$ values in eq 3, we estimate energy gaps $\Delta E^{ht}_{metal\rightarrow cof}$ for metal-to-cofactor hole injection at zero metal−cofactor bias (q refers to the cofactor charge prior to its oxidation). Analogous estimates for metal-to-cofactor electron injection are shown in the Supporting Information. We use a range of dielectric constants, as in the previous computations. $\Delta E^{ht}_{metal\rightarrow cof}$ gives an indication of the driving force for metal-to-cofactor charge transfer at zero bias only if the cofactor is not in direct contact with the metal, i.e., if there is no hybridization with the metal and no significant image charges. For a gold electrode with $E^{Au}_{Fermi} \simeq -5.1$ eV[84,85] (Figure 5), we predict that for most structures $\Delta E^{ht}_{metal\rightarrow cof}(q) < 0$, if the cofactor has total charge of $q = -1, -2, -3$. In particular

$$|\Delta E^{ht}_{metal\rightarrow cof}(q=-1)| < |\Delta E^{ht}_{metal\rightarrow cof}(q=-2)| < |\Delta E^{ht}_{metal\rightarrow cof}(q=-3)|$$

. Also $|\Delta E^{ht}_{metal\rightarrow cof}|$ decreases with cofactor size (Tables S5−S7). However, for a neutral cofactor, $\Delta E^{ht}_{metal\rightarrow cof}(q=0) > 0$ (Table S4), suggesting that the reverse process is spontaneous, i.e., electron transfer from the metal to the $q = +1$ cofactor.

For the larger structures, the computed $\Delta E^{ht}_{metal\rightarrow cof}(q=-1)$ are too small to qualify a definite conclusion about the driving force, given the computational

https://doi.org/10.1021/acs.jpcb.4c08264
J. Phys. Chem. B 2025, 129, 2992−3006

errors and the approximation for E^{Au}_{Fermi}. For example, for structure 9 in Figure 4, $\Delta E^{ht}_{metal\rightarrow cof}(q=-1) = -0.09$ eV. For structure 12 in Figure 4, $\Delta E^{ht}_{metal\rightarrow cof}(q=-1) = +0.02$ eV, (less than K_BT), suggesting that electron injection from the metal to the neutral cofactor is equally likely as hole injection. In addition, although the driving force $\Delta E^{ht}_{metal\rightarrow cof}(q=0)$ is generally positive, indicating spontaneous electron injection from the metal to the $q = +1$ state of the cofactor, the minimum value can be small. For example, for structure 7 in Figure 3, $\Delta E^{ht}_{metal\rightarrow cof}(q=0) = 0.07$ eV and this value can be reversed to negative by applying a small bias. In summary, hole injection to the $q = -1,-2,-3$ charge states of the cofactor is likely at zero bias (with a higher driving force for $q = -2,-3$). For the neutral cofactor ($q = 0$), electron injection from the metal is more probable, although for some structures hole injection to the neutral cofactor can be induced by a small bias.

Tunneling Matrix Element for Hole Transfer Between Cofactors Mediated by Amino Acids. Our results for the −1/−2 and 0/−1 cofactor redox couples show that the AA bridge most likely presents an energy barrier greater than K_BT for bridge-mediated cofactor-to-cofactor hole transfer. In this situation, AA-mediated tunneling is the most probable transfer mechanism. Our aim of this work is to estimate upper bounds for the magnitude of the AA-mediated tunneling matrix element. The maximum values should arise from the minimum energy barrier, which occurs for the 0/−1 couple combined with a Trp bridge.

We first approximate an upper bound for the nearest-neighbor cofactor-Trp electronic coupling, $V_{cof,Trp}$, by using eq 8. To do this, we combine each Ni-cofactor structure with a Trp monomer using different orientations with respect to the cofactor (Section S6). We find $V^{max}_{cof,Trp} \simeq 0.10$ eV (Table S17). Assuming that there is a linear bridge with N AA's connecting the donor and acceptor cofactors, we approximate the tunneling matrix element by,[86]

$$T^{eff}_{D,A}(N) \simeq V_{D,1}\frac{1}{\Delta E_{1,D}}V_{1,2}\frac{1}{\Delta E_{2,D}}V_{2,3}\cdots V_{N-1,N}\frac{1}{\Delta E_{N,A}}V_{N,A} \quad (12)$$

In the equation above, $V_{i,i+1}$ are nearest-neighbor hole-transfer couplings and $\Delta E_{i,D} = E_i - E_D$ (assuming a D−A resonance conformation for which $E_D = E_A$). Equation 12 and the tunneling mechanism are valid if the ratios $|V|/\Delta E < 1$.[86] To estimate an upper bound for the effective coupling, all $|\Delta E_{i,D}|$ are set equal to the minimum energy gap we have computed for the 0/−1 couple, i.e, $\Delta E^{ht}_{min} \simeq 0.2$ eV ($\Delta E^{ht}_{cof\rightarrow Trp}$ for structure 12 in Figure 4). We also use the maximum value $V^{max}_{cof,Trp} \simeq 0.10$ eV for $V_{D,1}$ and $V_{N,A}$. Thus, the maximum value for the ratios $V_{D,1}/\Delta E_{1,D}$ and $V_{N,A}/\Delta E_{N,A}$ in eq 12 is less than unity, $r_{max} = |V^{max}_{cof,Trp}/\Delta E^{ht}_{min}| \simeq 0.5$, and eq 12 is applicable. The maximum effective cofactor-to-cofactor coupling for the 0/−1 couple, mediated by a single Trp, is equal to max $|T_{D,A}(1)| = |(V^{max}_{cof,Trp})^2/\Delta E^{ht}_{min}| \simeq 0.05$ eV. For a longer bridge ($N \geq 2$),

$$\max|T_{D,A}(N)| \simeq r^2_{max}\left(\frac{1}{\Delta E^{ht}_{min}}\right)^{N-2}\prod_{i=1}^{N-1}V_{i,i+1} \quad (13)$$

where $r_{max} = |V^{max}_{cof,Trp}/\Delta E^{ht}_{min}| \simeq 0.5$ and $|\Delta E^{ht}_{min}| \simeq 0.2$ eV. It is best to estimate the product of couplings in eq 13 by referring to examples of biological Trp chains, where such couplings have been computed from known structures, e.g., refs[37,41]. In these systems rms couplings usually vary from one to a few tens of meV. To obtain approximate upper bounds, we will set all $V_{i,i+1} = 10$ meV in the equation above, i.e., $|V_{i,i+1}/\Delta E^{ht}_{min}| = 0.05$, well within the range of validity of eq 12. We find that $\max|T_{D,A}(N)| \simeq 10^{-4}$ eV for $N = 2-3$, dropping by a factor of 5×10^{-2} for each additional AA. These values will be used in the following section to obtain upper estimates of cofactor-to-cofactor hole-transfer times for the case of tunneling-mediated transport, where the intervening AA's act as virtual intermediates for the transferring hole.

The above discussion assumes that the ratio $r = |V_{cof,Trp}/\Delta E^{ht}|$ does not approach unity due to fluctuations in the D(A)-bridge energy gap and the D(A)-bridge coupling. Namely, in the previous discussion, the minimum value $\Delta E^{ht}_{min} = 0.2$ eV for the 0/−1 couple (structure 9 in Figure 4) and the maximum value $V^{max}_{cof,Trp} = 0.1$ eV should both be interpreted as mean values after thermal averaging. The root-mean-square (rms) fluctuation in the energy gap is given by $\sigma_{\Delta E} \simeq \sqrt{2\lambda K_BT}$, where λ is the reorganization energy. Given the computed reorganization energies (Tables S1 and S2), we find that 0.1 eV $\leq \sigma_{\Delta E} \leq$ 0.2 eV at room temperature. This implies that thermal fluctuations can bring with significant probability the energy gap close to zero, even if the average is $\Delta E^{ht}_{min} = 0.2$ eV. In this case, the ratio r could approach unity if we assume a cofactor-AA geometry that gives an rms $V_{cof,Trp}$ of the order of 0.1 eV. In this situation, the transport mechanism for the 0/−1 redox couple for the structures with the lowest average ht energy gap of 0.2 eV (most positive reduction potentials of 0/−1 in Figure 5), could involve resonant transport mechanisms. Thus, the regime in the region $0 < \Delta E^{ht}_{cof\rightarrow Trp} < 0.2$ eV is labeled "intermediate" in Figure 5. In this regime, the magnitude of the rms coupling compared to the rms energy gap determines whether D(A)-bridge resonances are relevant to transport. The cofactor-protein relative geometry and its thermal fluctuations are critical in determining the rms coupling. Structures with low cofactor-AA rms coupling (much less than 0.1 eV) would support off-resonant hole-transport, whereas higher rms-coupling ones could support resonant mechanisms. For the +1/0 couple, we have shown that the average energy gaps $\Delta E^{ht}_{cof\rightarrow Trp}$ can be lower than 0.2 eV or even negative. This redox couple lies mostly in the region of resonant AA-mediated hole-transfer mechanisms in the sense that its reduction-potential range overlaps with several AA reduction potentials (Figure 5). However, some structures are within the intermediate region described above for the 0/−1 couple.

Simulations of Amino Acid-Mediated Hole Transfer Between Cofactors. We estimate the minima for the hole-hopping times between cofactors for two distinct regimes: (a) transport mediated by the connecting AA's that act as real hopping intermediates and (b) transport mediated by the connecting AA's that act as virtual intermediates (Figure 1). We use the approach discussed in the Theoretical Methods section (eqs 4−7) and assume a Trp bridge since it provides the lowest protein−cofactor average energy gap. The method

https://doi.org/10.1021/acs.jpcb.4c08264
J. Phys. Chem. B 2025, 129, 2992−3006

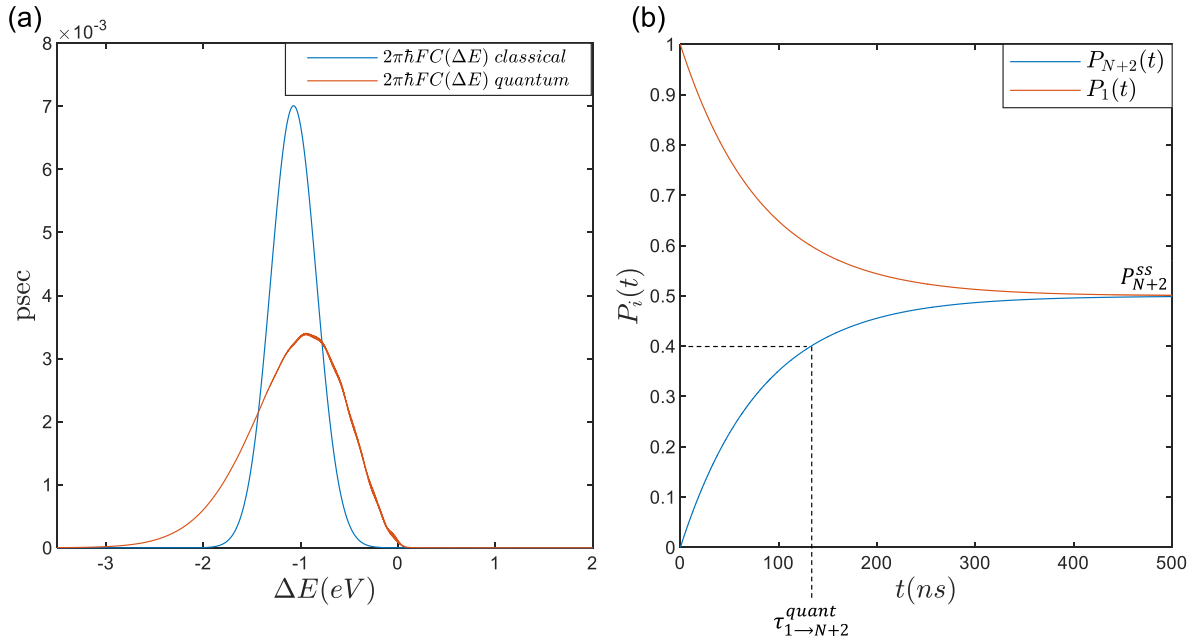

Figure 6. (a) Computed quantum (red line) and classical (blue line) Franck−Condon factors as a function of energy gap, (eq 4), for T = 300 K, $\hbar\Gamma$ = 0.001 eV for a pair of tryptophans. (b) $P_1(t)$ (red line) and $P_{N+2}(t)$ (blue line) are the time-dependent probabilities that the hole is at the donor and acceptor, respectively. The simulation describes thermally activated hopping through the connecting amino acids. These probabilities are obtained using eq 7 with T = 300 K and ΔV = 0 V. The donor and acceptor are cofactor structure 9 in Figure 4, and the bridge is a Trp triad (i.e., N = 3). The zero-bias Trp-cofactor energy gap is $\Delta E_{1,2}$ = 0.2 eV, the cofactor-Trp coupling is $V_{1,2} = V_{N+1,N+2}$ = 0.1 eV, and we use $V_{i,i+1}$ = 0.01 eV for the Trp−Trp couplings. From $P_{N+2}(t)$, we derive the overall donor-to-acceptor transfer time $\tau^{quant}_{1\to N+2}$ as the time it takes to reach 80% of the final steady-state acceptor probability.

Table 6. Theoretical Lower Bounds for Time Scales of Cofactor-to-Cofactor Hole Transfer at T = 300 K, Mediated by Themal Hopping Through a Bridge of Three Trp Amino Acids (Figure 1)[ab]

T = 300 K	ΔV = 0.0 V		ΔV = −0.5 V	
$\Delta E^{ht}_{cof\to Trp}$ (eV)	$\tau^{quant}_{1\to N+2}$ (nsec)	$\tau^{class}_{1\to N+2}$ (nsec)	$\tau^{quant}_{1\to N+2}$ (nsec)	$\tau^{class}_{1\to N+2}$ (nsec)
0.2	210 (170)	1×10^5	0.50 (0.50)	110
0.1	5 (4)	3×10^3	0.10 (0.05)	12
0.0	0.20 (0.20)	122	0.05 (0.04)	10

[a]Nonadiabatic Marcus theory is used for the computation of the rates ("quant" and "class" denote computations using the quantum and classical Franck-Condon factors). The cofactor chosen for the computation of the Franck-Condon factors is structure 5 in Figure 3, and the computations are done for the case of zero bias between the cofactors and a bias of −0.5 V. [b]The reported values in black (blue) are obtained using $\hbar\Gamma$ = 0.001 eV ($\hbar\Gamma$ = 0.01 eV) in eq 4.

builds an (N + 2)-site rate matrix where site i = 1 is a cofactor (initial hole donor), site N + 2 is the same cofactor (final hole acceptor). The remaining "bridge" sites i = 2−(N + 1) are Trp's. All rates $k_{i,i\pm1}$ are computed using Franck−Condon factors $FC_{quant}(\Delta E_{i,i\pm1})$ in eqs 4 and 6. The normal-mode frequencies ω_a and the corresponding λ_α are computed at the ab initio level for both the cofactors and the AA's. The rate equations are solved to obtain the probability of hole transfer to any of the sites, $P_i(t)$, given that initially the hole is in site 1, i.e., $P_{i,1}(t = 0) = \delta_{i,1}$. From $P_{N+2}(t)$ we derive the overall donor-to-acceptor transfer time $\tau^{quant}_{1\to N+2} = \tau^{quant}_{D\to A}$. It is defined as the time it takes to reach a significant percentage of the final steady-state acceptor probability P^{ss}_{N+2} (Figure 6). In the figure, we make the choice of 80%, but the results do not change significantly for a higher percentage. Further, we repeat the computations by replacing $FC_{quant}(\Delta E_{i,i\pm1})$ with the classical Franck−Condon factor using the sum of the total computed inner-sphere reorganization energies for i and $i \pm 1$, i.e.,

$$FC_{class}(\Delta E_{i,i\pm1}) = (\sqrt{4\pi\lambda_{i\pm1,i}K_BT})^{-1} \exp(-(\Delta E_{i\pm1,i} + \lambda_{i\pm1,i})^2/4\lambda_{i\pm1,i}K_BT)$$

where $\lambda_{i\pm1,i} = \lambda_i^{tot} + \lambda_{i\pm1}^{tot}$ and $\lambda_i^{tot} = \sum_\alpha \lambda_\alpha$. In this case, the transfer time is defined the same way as in the quantum case and it is denoted $\tau^{class}_{1\to N+2} = \tau^{class}_{D\to A}$.

Below, we show results for Trp triad parameters that would correspond to bridge lengths of 1−1.5 nm.[34−38] In all cases the cofactor-to-cofactor hole-transfer time ($\tau^{quant}_{1\to N+2}$) is computed as a function of overall bias ΔV (between sites 1 and N + 2), starting at zero bias. For the nearest-neighbor coupling parameters, we use the values discussed above, i.e., $V_{1,2} = V_{N+1,N+2}$ = 0.1 eV for the maximum cofactor-Trp coupling, and $V_{i,i+1}$ = 10 meV (i = 2 to N) for the Trp−Trp couplings. The zero-bias Trp-cofactor energy gaps $\Delta E_{2,1} = -\Delta E_{N+2,N+1}$ are varied from the minimum value computed for the 0/−1 couple, $\Delta E^{ht}_{min} \simeq$ 0.2 eV, to 0 eV (this range is possible for the

https://doi.org/10.1021/acs.jpcb.4c08264
J. Phys. Chem. B 2025, 129, 2992−3006

+1/0 couple). We do not consider negative zero-bias energy gaps because, in this regime, the Trp's would be the hole traps rather than the cofactors (a case that is not considered in this work, as it could slowdown cofactor-to-cofactor transport). The zero-bias Trp−Trp energy gaps are all set to zero, $\Delta E_{i+1,i} = 0eV$ for $i = 2$ to N.

Tables S1 and S2 show the computed total inner-sphere reorganization energies for different cofactor structures and AA side chains. An important conclusion of our computations is that the cofactor inner-sphere reorganization energies are very small for all cofactor types and redox couples (maximum value ≈0.1 eV and minimum value ≈0.025 eV). For example, in 3-Ni structure 9 in Figure 4, a 3-Ni structure has the lowest inner-sphere reorganization energy $\lambda = 0.025$ eV (order of K_BT (300 K)). The total computed inner-sphere reorganization energies for the AA side chains such as Tyr and Trp are in the range 0.3−0.5 eV.

Table 6 shows the computed ht time scales at different biases, using structure 5 in Figure 3 and a bridge of three Trp amino acids. The inner-sphere reorganization energies of the D (A) cofactor and each Trp are $\lambda^{tot}_{i=1(N+2)} = 0.07$ eV and $\lambda^{tot}_{i=2-N+1} = 0.50$ eV, respectively. Hence the total inner sphere reorganization energies for the D(A)-Trp rates and for the Trp−Trp rates are, respectively, $\lambda_{2,1} = \lambda_{N+2,N+1} = 0.57$ eV and $\lambda_{i+1,i} = 1$ eV ($i = 2, N$). The tabulated values are obtained using vibrational relaxation times, Γ^{-1} in eq 4, in the range of psec−100 fsec ($\hbar\Gamma = 0.001 - 0.01$ eV). At zero bias ($\Delta V = 0$ V), the quantum transfer times for $\hbar\Gamma = 0.001$ eV vary from $\tau^{quant}_{D\to A} = 210$ nsec at $\Delta E^{ht}_{cof\to Trp} = 0.2$ eV to $\tau^{quant}_{D\to A} = 0.2$ nsec at $\Delta E^{ht}_{cof\to Trp} = 0$ eV. The classical transfer times are much slower, with $\tau^{class}_{D\to A} = 100\ \mu$sec at $\Delta E^{ht}_{cof\to Trp} = 0.2$ eV to $\tau^{class}_{D\to A} = 122$ nsec at $\Delta E^{ht}_{cof\to Trp} = 0$ eV . Hole transfer become faster for $\Delta V = -0.5$ V, with $\tau^{quant}_{D\to A} = 0.5 - 0.05$ nsec and $\tau^{class}_{D\to A} = 110$ nsec − 10 nsec. Very similar time scales are obtained for $\hbar\Gamma = 0.01$ eV, and for other cofactor structures (Table S20). The case of two Trp's also gives similar results (Tables S18 and S19). In these simulations, the Trp−Trp steps are rate-limiting and determine the overall transfer times. This is because the total inner sphere reorganization energy for the Trp−Trp hopping step is the highest (1 eV). The differences between quantum and classical transfer times is due to the fact that most of the modes that contribute to the inner-sphere reorganization energy in Trp are nonclassical at room temperature, i.e., $\hbar\omega_\alpha > K_BT_{room}$ (Figures 6a and S1). Therefore, the fully classical approximation is not valid and underestimates the Trp−Trp rates. The computed quantum Trp−Trp rates are of the order of tens of picoseconds, close to measured Trp−Trp rates with Trp chains in photolyases and cryptochromes.[38] In contrast, the classical-approximation rates are nanoseconds to tens of nanoseconds.

The smallest possible protein bridge is composed of a single Trp. We also consider this case of AA-mediated hopping for the sake of comparison with Table 6. Using the maximum cofactor-Trp coupling of 0.1 eV and $\hbar\Gamma = 0.001$ eV, we find that $\tau^{quant}_{D\to A} = 30$ psec for $\Delta V = 0$ V, $\Delta E^{ht}_{cof\to Trp} = 0.2$ eV. All lower energy gaps for the single-Trp case give rates that are on the order of the vibrational relaxation times (Section S7) and should not be considered as valid within the theory we use. This is because nonadiabatic, thermally equilibrated quantum and classical Marcus models do not apply, since these models assume vibrational equilibrium prior to charge transfer.

We now consider the situation where the amino acids act as virtual intermediates. This mechanism may compete with amino acid hopping described above for the lower average energy gaps of the 0/−1 couple (0.2 eV). The corresponding rate is labeled k_{tunn} in Figure 1. For a Trp triad with $\Delta E^{ht}_{cof\to Trp} = 0.2$ eV we estimated in the previous section a maximum value of the effective coupling mediated by the bridge, $\max|T_{D,A}| \sim 10^{-4}$ eV (eq 13). Using structure 5 in Figure 3 or structure 9 in Figure 4 as examples, we find $\tau^{quant}_{tun} = 1/k_{tun} = 1 - 10$ nsec at zero bias between cofactors. Therefore, in the case of the 0/−1 couple and for bridge lengths on the order of 1 nm the maximum theoretical value for the transfer time of AA-mediated tunneling at zero bias can be shorter than the corresponding time for AA-mediated hopping (200 nsec in Table 6). This occurs because the inner-sphere reorganization energy for tunneling is the sum of the total reorganization energies of the D and A cofactors, $\lambda^{tot}_D+\lambda^{tot}_A = 0.14$ eV for structure 5 ($\lambda^{tot}_D+\lambda^{tot}_A = 0.05$ eV for structure 9) . The Trps's are not real intermediates and there are no Trp−Trp hopping steps that slow down transport due to the high reorganization energy of 1 eV (as in the AA-mediated hopping mechanism).

The above quantum simulations use only the inner-sphere reorganization energies for cofactors and AA's, computed at the ab initio level. The majority of these modes are nonclassical at room temperature, i.e., $\hbar\omega_\alpha > K_BT_{300\ K}$ (Tables S1 and S2, and Figure S1). However, in any protein−cofactor assembly, there will also be a high number of lower-frequency collective modes that are classical at room temperature with $\hbar\omega_\alpha < K_BT_{300\ K}$. The effect of such modes can only be described here phenomenologically, since we have no structural information about such assemblies. We do this in the Section S8 by using a mixed quantum−classical theory,[87] where the classical modes are introduced via an outer sphere reorganization energy λ_{out}. The computed quantum-classical transfer times $\tau^{quant-class}_{D\to A}$ (Table S21) become larger than the $\tau^{quant}_{D\to A}$ as λ_{outer} is increased. Therefore, the $\tau^{quant}_{D\to A}$ described above are lower bounds for the transfer times that are relevant to systems with outer-sphere reorganization energies that are much lower than the inner-sphere ones.

In summary, for a pair of cofactors connected by a typical Trp triad of approximately 1−1.5 nm length, the theoretical minimum ht times between the cofactors ($\lambda_{outer} = 0$), mediated by hopping through real AA intermediates, is in the range of hundreds of nsec for the redox couple 0/−1 to hundreds of psec for the redox couple +1/0. These numbers relate to identical donor and acceptor cofactors, with zero bias between them. The longer times for the 0/−1 couple are related to the minimum estimated Trp-cofactor energy gap of $\Delta E^{ht}_{cof\to Trp} = 0.2$ eV. The shortest times for the +0/1 couple are associated with a Trp-cofactor energy gap of $\Delta E^{ht}_{cof\to Trp} = 0$ eV. Shorter time scales (1−10 nsec) can be achieved for $\Delta E^{ht}_{cof\to Trp} = 0.2$ eV if the Trp-triad is a tunneling barrier. This is because the reorganization energies of the cofactors are much lower than Trp. To achieve shorter ht times, the bridge length would have to be reduced. In the case of the cable-bacteria experiments in refs[7−9], the estimated

https://doi.org/10.1021/acs.jpcb.4c08264
J. Phys. Chem. B 2025, 129, 2992−3006

voltage drop between adjacent cofactors is much less than K_BT. Therefore, the computed times more relevant to these experiments are those for $\Delta V = 0$ V. These times cannot explain the experimental room-temperature conductivities of 0.1 S/cm (or higher) in cable bacteria. For the 0.1 S/cm conductivities, the fitted rates are 0.1−1 psec^{-1} for estimates of cofactor center-to-center distances of 0.26−3.3 nm.[9]

CONCLUSIONS

Motivated by the recent discovery that Ni-bis(dithiolene) molecules are redox cofactors in cable bacteria charge-transfer chains, we explore the question of how such molecules would perform as redox components in protein wires, artificial, or biological. We focus on the case where nearest-neighbor cofactors are connected by an amino acid bridge. In this situation, the bridge plays an active role in charge transfer by providing real or virtual amino acid intermediates for transfer. The Ni-bis(dithiolene) structures are planar, and their redox-active orbitals are noninnocent, containing substantial sulfur and ligand character in addition to nickel. Therefore, their ionization potentials can be tuned by ligand substitutions, and their planar structures allow for extensive and variable interactions with surrounding amino acids. In addition, voltametry experiments on different Ni-bis(dithiolene) structures in a variety of solvents show that these molecules support several redox couples (e.g., + 1/0, 0/−1, and −1/−2). These characteristics suggest that Ni-bis(dithiolene) structures are versatile redox cofactors that can be used in protein wires to tune charge-transfer speeds. We study several single-nickel and multinickel cofactor structures related to voltametry and conductivity experiments on synthetic systems. For these structures, we consider the redox couples +1/0, 0/−1, −1/−2, and −2/−3. Given the lack of atomic-level information on protein−cofactor interactions, our results are approximate, and we look only for qualitative trends.

We show that the cofactor reduction potential becomes more negative as the redox couple changes from +1/0 to −2/−3. For any redox couple, the reduction potential is tunable over a range of 1 V or more (Figure 5), with the multinickel structures having the more positive potentials. In addition, we find that the inner-sphere reorganization energies of all structures are low ($\lambda \leq 0.1$ eV). The reduction potentials overlap with the potentials of many biological redox proteins (Figure 5). For all of the structures we have studied, the redox couples −2/−3, −1/−2, and 0/−1 may reduce O_2 (for +1/0 only some structures could). Therefore, Ni-bis(dithiolene) protein systems can be compatible with biological electron-transfer chains. In relation to cable bacteria that oxidize H_2S to reduce O_2, we show that the −1/−2, 0/−1, and +1/0 couples could oxidize H_2S (−2/−3 is likely not an H_2S oxidant).

We also compute, using quantum nonadiabatic rate theory, approximate upper bounds for protein-mediated hole-transfer rates between nearest-neighbor cofactors for a cofactor-to-cofactor distance of ≈1.5 nm and a bridge comprised of Trp amino acids. Trp is chosen because it has the lowest reduction potential for the amino acid cation (together with Tyr). We find that the +1/0 redox couple would support fast amino acid-mediated transport because amino acid-cofactor energy gaps for hole transfer can be zero for many of the cofactor structures, giving real amino acid intermediates. The redox couple 0/−1 would also be a good candidate for fast transport, as we find structures that give low amino acid-cofactor energy gaps of approximately 0.2 eV. The corresponding energy gaps for the −1/−2 redox couple are higher as compared to the 0/−1 redox couple (and even higher for the couple −2/−3). Therefore, the −2/−3 and −1/−2 couples are expected to support slower amino acid-mediated hole transport as compared to the others. The faster computed hole-transfer times using standard nonadiabatic rate theory are nsecs, for intercofactor distances of ≈1.5 nm and a Trp bridge. This timescale is much slower than the cofactor-to-cofactor transfer times in cable-bacteria, as estimated from experiments using center-to-center cofactor distances of 0.26−3.3 nm. Our results can serve as guidelines for designing protein wires with Ni-bis(dithiolene) redox cofactors and tunable charge transfer rates.

ASSOCIATED CONTENT

Supporting Information

The Supporting Information is available free of charge at https://pubs.acs.org/doi/10.1021/acs.jpcb.4c08264.

(1) Inner-sphere reorganization energies of cofactors and amino acid side chains, (2) protein-mediated cofactor-to-cofactor hole transfer, (3) hole injection from metal to cofactor, (4) protein-mediated cofactor-to-cofactor electron transfer, (5) electron injection from metal to cofactor, (6) computation of electronic couplings for different Ni-cofactor/tryptophan geometries, (7) simulations of amino acid-mediated hole transfer between cofactors, (8) the quantum case and the mixed quantum-classical case, and (9) ground state coordinates of Ni-bis(dithiolene) complexes (PDF)

AUTHOR INFORMATION

Corresponding Author

Spiros S. Skourtis − *Department of Physics, University of Cyprus, Nicosia 1678, Cyprus;* orcid.org/0000-0002-5834-248X; Email: skourtis@ucy.ac.cy

Author

Georgia Polycarpou − *Department of Physics, University of Cyprus, Nicosia 1678, Cyprus;* orcid.org/0000-0002-3352-4228

Complete contact information is available at: https://pubs.acs.org/10.1021/acs.jpcb.4c08264

Notes

The authors declare no competing financial interest.

ACKNOWLEDGMENTS

The authors thank the EIC Pathfinder project 101046719 PRINGLE for financial support and Dr. Stefani Valianti, and Profs. Filip Meysman, Herre van der Zant, and Han Remaut for helpful discussions.

REFERENCES

(1) Pfeffer, C.; Larsen, S.; Song, J.; Dong, M.; Besenbacher, F.; Meyer, R. L.; Kjeldsen, K. U.; Schreiber, L.; Gorby, Y. A.; El-Naggar, Y. M.; et al. Filamentous bacteria transport electrons over centimetre distances. *Nature* **2012**, *491*, 218−221.

(2) Meysman, F. J. Cable bacteria take a new breath using long-distance electricity. *Trends Microbiol.* **2018**, *26*, 411−422.

(3) Bjerg, J. T.; Boschker, H. T.; Larsen, S.; Berry, D.; Schmid, M.; Millo, D.; Tataru, P.; Meysman, F. J.; Wagner, M.; Nielsen, L. P.; et al. Long-distance electron transport in individual, living cable bacteria. *Proc. Natl. Acad. Sci. U. S. A.* **2018**, *115*, 5786−5791.

(4) Meysman, F. J.; Cornelissen, R.; Trashin, S.; Bonné, R.; Martinez, S. H.; van der Veen, J.; Blom, C. J.; Karman, C.; Hou, J.-L.; Eachambadi, R. T.; et al. A highly conductive fibre network enables centimetre-scale electron transport in multicellular cable bacteria. *Nat. Commun.* **2019**, *10*, 4120.
(5) Bonné, R.; Hou, J.-L.; Hustings, J.; Wouters, K.; Meert, M.; Hidalgo-Martinez, S.; Cornelissen, R.; Morini, F.; Thijs, S.; Vangronsveld, J.; et al. Intrinsic electrical properties of cable bacteria reveal an Arrhenius temperature dependence. *Sci. Rep.* **2020**, *10*, 19798.
(6) Boschker, H. T.; Cook, P. L.; Polerecky, L.; Eachambadi, R. T.; Lozano, H.; Hidalgo-Martinez, S.; Khalenkow, D.; Spampinato, V.; Claes, N.; Kundu, P.; et al. Efficient long-range conduction in cable bacteria through nickel protein wires. *Nat. Commun.* **2021**, *12*, 3996.
(7) van der Veen, J. R.; Martinez, S. H.; Wieland, A.; De Pellegrin, M.; Verweij, R.; Blanter, Y. M.; van der Zant, H. S.; Meysman, F. J. Quantum-assisted electron transport in microbial protein wires across macroscopic distances. *arXiv*, **2023**, .
(8) van der Veen, J. *The charge transport mechanism in cable bacteria* Ph.D. thesis. Delft University of Technology; 2024.
(9) van der Veen, J. R.; Valianti, S.; van der Zant, H. S.; Blanter, Y. M.; Meysman, F. J. A model analysis of centimeter-long electron transport in cable bacteria. *Phys. Chem. Chem. Phys.* **2024**, *26*, 3139−3151.
(10) Yang, T.; Chavez, M. S.; Niman, C. M.; Xu, S.; El-Naggar, M. Y. Long-distance electron transport in multicellular freshwater cable bacteria. *eLife* **2024**, *12*, RP91097.
(11) van der Veen, J. R.; Hidalgo Martinez, S.; Wieland, A.; De Pellegrin, M.; Verweij, R.; Blanter, Y. M.; van der Zant, H. S.; Meysman, F. J. Temperature-Dependent Characterization of Long-Range Conduction in Conductive Protein Fibers of Cable Bacteria. *ACS Nano* **2024**, *18*, 32878−32889.
(12) El-Naggar, M. Y.; Wanger, G.; Leung, K. M.; Yuzvinsky, T. D.; Southam, G.; Yang, J.; Lau, W. M.; Nealson, K. H.; Gorby, Y. A. Electrical transport along bacterial nanowires from Shewanella oneidensis MR-1. *Proc. Natl. Acad. Sci. U. S. A.* **2010**, *107*, 18127−18131.
(13) Xu, S.; Barrozo, A.; Tender, L. M.; Krylov, A. I.; El-Naggar, M. Y. Multiheme cytochrome mediated redox conduction through Shewanella oneidensis MR-1 cells. *J. Am. Chem. Soc.* **2018**, *140*, 10085−10089.
(14) Polizzi, N. F.; Skourtis, S. S.; Beratan, D. N. Physical constraints on charge transport through bacterial nanowires. *Faraday Discuss.* **2012**, *155*, 43−61.
(15) Breuer, M.; Rosso, K. M.; Blumberger, J. Electron flow in multiheme bacterial cytochromes is a balancing act between heme electronic interaction and redox potentials. *Proc. Natl. Acad. Sci. U. S. A.* **2014**, *111*, 611−616.
(16) Wang, F.; Gu, Y.; O'Brien, J. P.; Sophia, M. Y.; Yalcin, S. E.; Srikanth, V.; Shen, C.; Vu, D.; Ing, N. L.; Hochbaum, A. I.; et al. Structure of microbial nanowires reveals stacked hemes that transport electrons over micrometers. *Cell* **2019**, *177*, 361−369.E10.
(17) Guberman-Pfeffer, M. J. Assessing thermal response of redox conduction for anti-Arrhenius kinetics in a microbial cytochrome nanowire. *J. Phys. Chem. B* **2022**, *126*, 10083−10097.
(18) Smets, B.; Boschker, H. T.; Wetherington, M. T.; Lelong, G.; Hidalgo-Martinez, S.; Polerecky, L.; Nuyts, G.; De Wael, K.; Meysman, F.J. Multi-wavelength Raman microscopy of nickel-based electron transport in cable bacteria. *Front. Microbiol.* **2024**, *15*, 1208033.
(19) Petrenko, T.; Ray, K.; Wieghardt, K. E.; Neese, F. Vibrational markers for the open-shell character of transition metal bis-dithiolenes: an infrared, resonance Raman, and quantum chemical study. *J. Am. Chem. Soc.* **2006**, *128*, 4422−4436.
(20) Kato, R. Conducting metal dithiolene complexes: Structural and electronic properties. *Chem. Rev.* **2004**, *104*, 5319−5346.
(21) Liu, Z.; Liu, T.; Savory, C. N.; Jurado, J. P.; Reparaz, J. S.; Li, J.; Pan, L.; Faul, C. F.; Parkin, I. P.; Sankar, G.; et al. Controlling the thermoelectric properties of organometallic coordination polymers via ligand design. *Adv. Funct. Mater.* **2020**, *30*, 2003106.
(22) Sun, Y.; Sheng, P.; Di, C.; Jiao, F.; Xu, W.; Qiu, D.; Zhu, D. Organic Thermoelectric Materials and Devices Based on p- and n-Type Poly(metal 1,1,2,2-ethenetetrathiolate)s. *Adv. Mater.* **2012**, *24*, 932−937.
(23) Kobayashi, Y.; Jacobs, B.; Allendorf, M. D.; Long, J. R. Conductivity, doping, and redox chemistry of a microporous dithiolene-based metal- organic framework. *Chem. Mater.* **2010**, *22*, 4120−4122.
(24) Tetsuya, K.; Ryota, S.; Tetsuro, K.; Tigmansu, P.; Naoya, F.; Ken, H.; Takahiro, S.; Zhengfei, W.; Toru, H.; Kyoko, I.; et al. Redox Control and High Conductivity of Nickel Bis (dithiolene) Complex π-Nanosheet: A Potential Organic Two-Dimensional Topological Insulator. *J. Am. Chem. Soc.* **2014**, *136*, 14357−14360.
(25) Eisenberg, R.; Gray, H. B. Noninnocence in metal complexes: A dithiolene dawn. *Inorg. Chem.* **2011**, *50*, 9741−9751.
(26) Szilagyi, R. K.; Lim, B. S.; Glaser, T.; Holm, R. H.; Hedman, B.; Hodgson, K. O.; Solomon, E. I. Description of the ground state wave functions of Ni dithiolenes using sulfur K-edge X-ray absorption spectroscopy. *J. Am. Chem. Soc.* **2003**, *125*, 9158−9169.
(27) Dey, A.; Jeffrey, S. P.; Darensbourg, M.; Hodgson, K. O.; Hedman, B.; Solomon, E. I. Sulfur K-edge XAS and DFT studies on NiII complexes with oxidized thiolate ligands: implications for the roles of oxidized thiolates in the active sites of Fe and Co nitrile hydratase. *Inorg. Chem.* **2007**, *46*, 4989−4996.
(28) Ray, K.; Weyhermüller, T.; Neese, F.; Wieghardt, K. Electronic Structure of Square Planar Bis(benzene-1,2-dithiolato)metal Complexes $[M(L)_2]^z$ (z = 2,1,0;M = *Ni,Pd,Pt,Cu,Au*): An Experimental, Density Functional, and Correlated ab Initio Study. *Inorg. Chem.* **2005**, *44*, 5345−5360.
(29) Rovira, C.; Novoa, J. J.; Mozos, J.-L.; Ordejón, P.; Canadell, E. First-principles study of the neutral molecular metal $Ni(tmdt)_2$. *Phys. Rev. B* **2002**, *65*, 081104.
(30) Machata, P.; Herich, P.; Luspai, K.; Bucinsky, L.; Soralova, S.; Breza, M.; Kozisek, J.; Rapta, P. Redox reactions of nickel, copper, and cobalt complexes with "noninnocent" dithiolate ligands: combined in situ spectroelectrochemical and theoretical study. *Organometallics* **2014**, *33*, 4846−4859.
(31) Sørensen, M. L.; Sanders, B. C.; Hicks, L. P.; Rasmussen, M. H.; Vishart, A. L.; Kongsted, J.; Winkler, J. R.; Gray, H. B.; Hansen, T. Hole hopping through cytochrome P450. *J. Phys. Chem. B* **2020**, *124*, 3065−3073.
(32) Takematsu, K.; Williamson, H. R.; Nikolovski, P.; Kaiser, J. T.; Sheng, Y.; Pospíšil, P.; Towrie, M.; Heyda, J.; Hollas, D.; Záliš, S.; et al. Two tryptophans are better than one in accelerating electron flow through a protein. *ACS Cent. Sci.* **2019**, *5*, 192−200.
(33) Melčák, M.; šebesta, F.; Heyda, J.; Gray, H. B.; Záliš, S.; Vlček, A. Tryptophan to Tryptophan Hole Hopping in an Azurin Construct. *J. Phys. Chem. B* **2024**, *128*, 96−108.
(34) Kao, Y.-T.; Tan, C.; Song, S.-H.; Öztürk, N.; Li, J.; Wang, L.; Sancar, A.; Zhong, D. Ultrafast dynamics and anionic active states of the flavin cofactor in cryptochrome and photolyase. *J. Am. Chem. Soc.* **2008**, *130*, 7695−7701.
(35) Kao, Y.-T.; Saxena, C.; He, T.-F.; Guo, L.; Wang, L.; Sancar, A.; Zhong, D. Ultrafast dynamics of flavins in five redox states. *J. Am. Chem. Soc.* **2008**, *130*, 13132−13139.
(36) Lüdemann, G.; Woiczikowski, P. B.; Kubar, T.; Elstner, M.; Steinbrecher, T. B. Charge transfer in E. coli DNA photolyase: Understanding polarization and stabilization effects via QM/MM simulations. *J. Phys. Chem. B* **2013**, *117*, 10769−10778.
(37) Woiczikowski, P. B.; Steinbrecher, T.; Kubar, T.; Elstner, M. Nonadiabatic QM/MM simulations of fast charge transfer in Escherich ia coli DNA photolyase. *J. Phys. Chem. B* **2011**, *115*, 9846−9863.
(38) Zhong, D. Electron transfer mechanisms of DNA repair by photolyase. *Arch. Biochem. Biophys.* **2015**, *66*, 691−715.
(39) Winkler, J. R.; Gray, H. B. Electron flow through metalloproteins. *Chem. Rev.* **2014**, *114*, 3369−3380.

https://doi.org/10.1021/acs.jpcb.4c08264
J. Phys. Chem. B 2025, 129, 2992−3006

(40) Shih, C.; Museth, A. K.; Abrahamsson, M.; Blanco-Rodriguez, A. M.; Bilio, A. J. D.; Sudhamsu, J.; Crane, B. R.; Ronayne, K. L.; Towrie, M.; Vlček, A.; et al. Tryptophan-accelerated electron flow through proteins. *Science* **2008**, *320*, 1760−1762.
(41) Polizzi, N. F.; Migliore, A.; Therien, M. J.; Beratan, D. N. Defusing redox bombs? *Proc. Natl. Acad. Sci. U. S. A.* **2015**, *112*, 10821−10822.
(42) Gray, H. B.; Winkler, J. R. Hole hopping through tyrosine/tryptophan chains protects proteins from oxidative damage. *Proc. Natl. Acad. Sci. U. S. A.* **2015**, *112*, 10920−10925.
(43) Mahmoudi, L.; Kissner, R.; Nauser, T.; Koppenol, W. H. Electrode potentials of L-tryptophan, L-tyrosine, 3-nitro-L-tyrosine, 2, 3-difluoro-L-tyrosine, and 2, 3, 5-trifluoro-L-tyrosine. *Biochemistry* **2016**, *55*, 2849−2856.
(44) Szabo, A.; Ostlund, N. *Modern Quantum Chemistry: introduction to Advanced Electronic Structure Theory*; Dover Publications, 1996.
(45) Amb, C. M.; Heth, C. L.; Evenson, S. J.; Pokhodnya, K. I.; Rasmussen, S. C. Thiophene-Fused Nickel Dithiolenes: A Synthetic Scaffold for Highly Delocalized π-Electron Systems. *Inorg. Chem.* **2016**, *55*, 10978−10989.
(46) Uzelac, E. J.; Rasmussen, S. C. Thiophene-Extended Nickel Thiazoledithiolene: π-Extended Fused-Ring Metal Dithiolenes with Stabilized Frontier Orbitals. *Eur. J. Inorg. Chem.* **2017**, *2017*, 3878−3883.
(47) Kean, C. L.; Pickup, P. G. A low band gap conjugated metallopolymer with nickel bis(dithiolene) crosslinks. *Chem. Commun.* **2001**, *9*, 815−816.
(48) Bui, T.-T.; Garreau-de Bonneval, B.; Moineau-Chane Ching, K. I. Synthesis and preliminary physical properties of new neutral tetraalkoxy-substituted nickel bis(1,2-dithiolene) complexes. *New J. Chem.* **2010**, *34*, 337−347.
(49) Kean, C. L.; Miller, D. O.; Pickup, P. G. Thiophene-substituted nickel dithiolene complexes. Precursors for low band gap conjugated metallopolymers. *J. Mater. Chem.* **2002**, *12*, 2949−2956.
(50) Li, L.; Li, C.; Zhang, Z.; Alexov, E. On the dielectric "constant" of proteins: smooth dielectric function for macromolecular modeling and its implementation in DelPhi. *J. Chem. Theory And Comput.* **2013**, *9*, 2126−2136.
(51) Becke, A. D. Density functional calculations of molecular bond energies. *J. Chem. Phys.* **1986**, *84*, 4524−4529.
(52) Perdew, J. P. Density-functional approximation for the correlation energy of the inhomogeneous electron gas. *Phys. Rev. B* **1986**, *33*, 8822−8824.
(53) Schäfer, A.; Huber, C.; Ahlrichs, R. Fully optimized contracted Gaussian basis sets of triple zeta valence quality for atoms Li to Kr. *J. Chem. Phys.* **1994**, *100*, 5829−5835.
(54) Pantazis, D. A.; Chen, X.-Y.; Landis, C. R.; Neese, F. All-Electron Scalar Relativistic Basis Sets for Third-Row Transition Metal Atoms. *J. Chem. Theory Comput.* **2008**, *4*, 908−919.
(55) Neese, F. The ORCA program system. *Wiley Interdiscip. Rev.: Comput. Mol. Sci.* **2012**, *2*, 73−78.
(56) Neese, F. Software update: The ORCA program system—Version 5.0. *Comput. Mol. Biosci.* **2022**, *12*, No. e1606.
(57) Ray, K.; DeBeer George, S.; Solomon, E. I.; Wieghardt, K.; Neese, F. Description of the Ground-State Covalencies of the Bis(dithiolato) Transition-Metal Complexes from X-ray Absorption Spectroscopy and Time-Dependent Density-Functional Calculations. *Chem. Eur. J.* **2007**, *13*, 2783−2797.
(58) Waters, T.; Woo, H.-K.; Wang, X.-B.; Wang, L.-S. Probing the Intrinsic Electronic Structure of the Bis(dithiolene) Anions $[M(mnt)_2]^{1-}$ and $[M(mnt)_2]^{1-}$ (M = *Ni*, *Pd*, *Pt*;*mnt* = 1,2−$S_2C_2(CN)_2$) the Gas Phase by Photoelectron Spectroscopy. *J. Am. Chem. Soc.* **2006**, *128*, 4282−4291.
(59) Liu, X.; Hou, G.-L.; Wang, X.; Wang, X.-B. Negative Ion Photoelectron Spectroscopy Reveals Remarkable Noninnocence of Ligands in Nickel Bis(dithiolene) Complexes $[Ni(dddt)_2]$ and $[Ni(edo)_2]$. *J. Phys. Chem. A* **2016**, *120*, 2854−2862.
(60) Maluendes, S.A.; McLean, A.D.; Yamashita, K.; Herbst, E. Calculations on the competition between association and reaction for C3H(+) + H2. *J. Chem. Phys.* **1993**, *99*, 2812−2820.
(61) Bachler, V.; Olbrich, G.; Neese, F.; Wieghardt, K. Theoretical evidence for the singlet diradical character of square planar nickel complexes containing two o-semiquinonato type ligands. *Inorg. Chem.* **2002**, *41*, 4179−4193.
(62) Herebian, D.; Bothe, E.; Neese, F.; Weyhermüller, T.; Wieghardt, K. Molecular and Electronic Structures of Bis-(o-diiminobenzosemiquinonato)metal(II) Complexes (Ni, Pd, Pt), Their Monocations and -Anions, and of Dimeric Dications Containing Weak Metal-Metal Bonds. *J. Am. Chem. Soc.* **2003**, *125*, 9116−9128.
(63) Wong, Z. M.; Yong, X.; Deng, T.; Shi, W.; Wu, G.; Li, N.; Luo, H.-K.; Yang, S.-W. Neutral Antiaromatic Bis(1,2-dithiolene)-Chelated Nickel Complexes Bearing Multiradical Characters. *J. Phys. Chem. A* **2022**, *126*, 5552−5558.
(64) Becke, A. D. A new mixing of Hartree−Fock and local density-functional theories. *J. Chem. Phys.* **1993**, *98*, 1372−1377.
(65) Yu, W.; Liang, L.; Lin, Z.; Ling, S.; Haranczyk, M.; Gutowski, M. Comparison of some representative density functional theory and wave function theory methods for the studies of amino acids. *J. Comput. Chem.* **2009**, *30*, 589−600.
(66) Barone, V.; Cossi, M. Quantum Calculation of Molecular Energies and Energy Gradients in Solution by a Conductor Solvent Model. *J. Phys. Chem. A* **1998**, *102*, 1995−2001.
(67) Seldenthuis, J. S.; van der Zant, H. S. J.; Ratner, M. A.; Thijssen, J. M. Vibrational Excitations in Weakly Coupled Single-Molecule Junctions: A Computational Analysis. *ACS Nano* **2008**, *2*, 1445−1451.
(68) Ruhoff, P. T.; Ratner, M. A. Algorithms for computing Franck−Condon overlap integrals. *J. Quantum Chem.* **2000**, *77*, 383−392.
(69) Sando, G. M.; Spears, K. G. Ab Initio Computation of the Duschinsky Mixing of Vibrations and Nonlinear Effects. *J. Phys. Chem. A* **2001**, *105*, 5326−5333.
(70) Te Velde, G.; Bickelhaupt, F. M.; Baerends, E. J.; Fonseca Guerra, C.; van Gisbergen, S. J. A.; Snijders, J. G.; Ziegler, T. Chemistry with ADF. *J. Comput. Chem.* **2001**, *22*, 931−967.
(71) Senthilkumar, K.; Grozema, F. C.; Bickelhaupt, F. M.; Siebbeles, L. D. A. Charge transport in columnar stacked triphenylenes: Effects of conformational fluctuations on charge transfer integrals and site energies. *J. Chem. Phys.* **2003**, *119*, 9809−9817.
(72) Senthilkumar, K.; Grozema, F. C.; Guerra, C. F.; Bickelhaupt, F. M.; Lewis, F. D.; Berlin, Y. A.; Ratner, M. A.; Siebbeles, L. D. A. Absolute Rates of Hole Transfer in DNA. *J. Am. Chem. Soc.* **2005**, *127*, 14894−14903.
(73) Close, D. M. Calculated vertical ionization energies of the common α-amino acids in the gas phase and in solution. *J. Phys. Chem. A* **2011**, *115*, 2900−2912.
(74) Guo, C.; Yu, X.; Refaely-Abramson, S.; Sepunaru, L.; Bendikov, T.; Pecht, I.; Kronik, L.; Vilan, A.; Sheves, M.; Cahen, D. Tuning electronic transport via hepta-alanine peptides junction by tryptophan doping. *Proc. Natl. Acad. Sci. U. S. A.* **2016**, *113*, 10785−10790.
(75) Tyson, K. J.; Davis, A. N.; Norris, J. L.; Bartolotti, L. J.; Hvastkovs, E. G.; Offenbacher, A. R. Impact of local electrostatics on the redox properties of tryptophan radicals in azurin: Implications for redox-active tryptophans in proton-coupled electron transfer. *J. Phys. Chem. Lett.* **2020**, *11*, 2408−2413.
(76) Tyson, K.; Tangtartharakul, C. B.; Zeug, M.; Findling, N.; Haddy, A.; Hvastkovs, E.; Choe, J.-Y.; Kim, J. E.; Offenbacher, A. R. Electrochemical and Structural Study of the Buried Tryptophan in Azurin: Effects of Hydration and Polarity on the Redox Potential of W48. *J. Phys. Chem. B* **2023**, *127*, 133−143.
(77) Bard, A. J.; Faulkner, L. R. *Electrochemical methods: Fundamentals and applications*, 2nded.; John Wiley & Sons, 2022.
(78) Pavlishchuk, V. V.; Addison, A. W. Conversion constants for redox potentials measured versus different reference electrodes in acetonitrile solutions at 25 C. *Inorg. Chim. Acta* **2000**, *298*, 97−102.

https://doi.org/10.1021/acs.jpcb.4c08264
J. Phys. Chem. B 2025, 129, 2992−3006

(79) Namazian, M.; Lin, C. Y.; Coote, M. L. Benchmark calculations of absolute reduction potential of ferricinium/ferrocene couple in nonaqueous solutions. *J. Chem. Theory Comput.* **2010**, *6*, 2721−2725.
(80) Liu, J.; Chakraborty, S.; Hosseinzadeh, P.; Yu, Y.; Tian, S.; Petrik, I.; Bhagi, A.; Lu, Y. Metalloproteins containing cytochrome, iron−sulfur, or copper redox centers. *Chem. Rev.* **2014**, *114*, 4366−4469.
(81) Bertini, I.; Gray, H. B.; Lippard, S. J.; Valentine, J. S. *Bioinorganic chemistry*; University science books, 1994.
(82) Da Silva, J. F.; Williams, R. J. P. *The biological chemistry of the elements: the inorganic chemistry of life*; Oxford University Press, 2001.
(83) Voet, D.; Pratt, C. W.; Voet, J. G. *Voet's principles of biochemistry*; John Wiley & Sons, 2018.
(84) Eastman, D. E. Photoelectric Work Functions of Transition, Rare-Earth, and Noble Metals. *Phys. Rev. B* **1970**, *2*, 1−2.
(85) Li, H.; Yu, H.; Quan, X.; Chen, S.; Zhang, Y. Uncovering the Key Role of the Fermi Level of the Electron Mediator in a Z-Scheme Photocatalyst by Detecting the Charge Transfer Process of WO_3-metal-gC_3N_4 (Metal = Cu, Ag, Au). *ACS Appl. Mater. Interfaces* **2016**, *8*, 2111−2119.
(86) Skourtis, S. S.; Beratan, D. N. Theories of structure−function relationships for bridge-mediated electron transfer reactions. *Adv. Chem. Phys.* **1999**, *106*, 377−452.
(87) May, V.; Kühn, O. *Charge and energy transfer dynamics in molecular systems*; John Wiley & Sons, 2023.

https://doi.org/10.1021/acs.jpcb.4c08264
J. Phys. Chem. B 2025, 129, 2992−3006